BRL-TR-3026 DTIC FILE COPY

(4)

TECHNICAL REPORT BRL-TR-3026

BRL

AD-A211 364

LARGE BLAST AND THERMAL SIMULATOR ADVANCED CONCEPT DRIVER DESIGN BY COMPUTATIONAL FLUID DYNAMICS

KLAUS O. OPALKA

AUGUST 1989

U.S. ARMY LABORATORY COMMAND

BALLISTIC RESEARCH LABORATORY
ABERDEEN PROVING GROUND, MARYLAND

UNCLASSIFIED
SECURITY CLASSIFICATION OF THIS PAGE

REPORT DOCUMENTATION PAGE

Form Approved OMB No. 0704-0188

1a. REPORT SECURITY CLASSIFICATION UNCLASSIFIED	1b. RESTRICTIVE MARKINGS NONE
2a. SECURITY CLASSIFICATION AUTHORITY	3. DISTRIBUTION/AVAILABILITY OF REPORT APPROVED FOR PUBLIC RELEASE; DISTRIBUTION UNLIMITED
2b. DECLASSIFICATION/DOWNGRADING SCHEDULE	
4. PERFORMING ORGANIZATION REPORT NUMBER(S) BRL-TR-3026	5. MONITORING ORGANIZATION REPORT NUMBER(S)
6a. NAME OF PERFORMING ORGANIZATION US Army Ballistic Research Laboratory 6b. OFFICE SYMBOL (If applicable) SLCBR-TB-B	7a. NAME OF MONITORING ORGANIZATION
6c. ADDRESS (City, State, and ZIP Code) ABERDEEN PROVING GROUND, MARYLAND 21005-5066	7b. ADDRESS (City, State, and ZIP Code)
8a. NAME OF FUNDING/SPONSORING ORGANIZATION US Army Harry Diamond Laboratory 8b. OFFICE SYMBOL (If applicable) SLCHD-NW-P	9. PROCUREMENT INSTRUMENT IDENTIFICATION NUMBER
8c. ADDRESS (City, State, and ZIP Code) 2800 Powder Mill Road Adelphi, MD 20783-1197	10. SOURCE OF FUNDING NUMBERS PROGRAM ELEMENT NO. 62120 PROJECT NO. AH25 TASK NO. WORK UNIT ACCESSION NO.

11. TITLE (Include Security Classification)
Large Blast & Thermal Simulator Advanced Concept Driver Design by Computational Fluid Dynamics

12. PERSONAL AUTHOR(S)
Klaus O. Opalka

13a. TYPE OF REPORT	13b. TIME COVERED	14. DATE OF REPORT (Year, Month, Day)	15. PAGE COUNT
Final	FROM FY87 TO FY89		

16. SUPPLEMENTARY NOTATION

17. COSATI CODES

FIELD	GROUP	SUB-GROUP
20	04	
01	01	

18. SUBJECT TERMS (Continue on reverse if necessary and identify by block number)
Computational fluid dynamics, CFD design studies, Large Blast Wave Simulators, Blast Wave Simulation, Large Blast/Thermal Simulators, LB/TS Design

19. ABSTRACT (Continue on reverse if necessary and identify by block number)

The construction of a large test facility has been proposed for simulating the blast and thermal environment resulting from nuclear explosions. This facility would be used to test the survivability and vulnerability of military equipment such as trucks, tanks and helicopters in a simulated thermal and blast environment, and to perform research into nuclear blast phenomenology. The proposed advanced design concepts, heating of driver gas and fast-acting throat valves for wave shaping, are described and the results of CFD studies to advance these new technical concepts for simulating decaying blast waves are reported.

20. DISTRIBUTION/AVAILABILITY OF ABSTRACT ☒ UNCLASSIFIED/UNLIMITED ☐ SAME AS RPT. ☐ DTIC USERS	21. ABSTRACT SECURITY CLASSIFICATION UNCLASSIFIED
22a. NAME OF RESPONSIBLE INDIVIDUAL Klaus O. Opalka	22b. TELEPHONE (Include Area Code) (301) 278-6036 22c. OFFICE SYMBOL SLCBR-TB-B

TABLE OF CONTENTS

LIST OF ILLUSTRATIONS

1. INTRODUCTION

Due to the increased emphasis on tactical nuclear forces there is a growing concern for the survivability of US weapon systems on a combined conventional/nuclear battlefield. This concern is reflected in a number of DoD instructions and Army procurement regulations requiring specific nuclear hardness levels on weapons systems. There are within the US Army alone over 150 systems with nuclear survivability requirements. The ban on above-ground nuclear testing forces the U. S. Army to look for alternative techniques in its effort to respond to the growing need for nuclear, blast/thermal survivability testing of military equipment.

There exist currently two techniques for testing the susceptibility of modern weapon systems to blast effects, one using high explosives (HE) in large quantities, and the other using special shock tunnels. The simulation of blast waves with high explosives requires large test areas and is limited to small yields ($\leq$20 kT). Because of the high cost, the high environmental impact and the low frequency of HE tests (one test per year) specialized shock tunnels, called blast wave simulators, have been studied with increasing interest in recent years.

Large blast wave simulators are basically shock tunnels whose cross-sectional areas vary along their lengths. They are large enough to accommodate full-sized tactical equipment such as trucks, tanks and helicopters and allow frequent and repeatable testing (e.g., two tests per week) of a weapon system at a small fraction of the cost of a field test. A few such facilities exist in Europe, e.g., in the United Kingdom at the Atomic Weapons Establishment (AWE), Foulness, and in Germany (FRG) at the Erprobungsstelle 52, Oberjettenberg. The largest such facility exists in France at the Centre d'Etudes de Gramat (CEG), but none is located on the North American continent. In response to this void, the Defense Audit Service has recommended that the Defense Nuclear Agency (DNA) develop a large blast/thermal simulator (LB/TS) for the U.S. Armed Forces. The U.S. Army is presently developing the concept of such a facility on behalf of the DNA. The U.S. Army Ballistic Research Laboratory (BRL) has taken the lead role in the development of the LB/TS for the U.S. Army Harry Diamond Laboratory (HDL).

Initially, the U.S. design studies were based on the Large Blast Simulator (LBS) at the CEG, France[1*] (Figure 1). However, the studies were extended over a broader range of shock overpressures and weapon yields[2] to cover those test conditions which were specified in the operating envelope but could not be simulated in the CEG facility. Parametric design studies[3] were performed to answer questions about the necessary size and the expected performance of such a facility simulating the required range of blast waves. Furthermore, studies of the effect of target blockage on target loading[4] indicated that a much larger cross-section would be needed in the test section to accommodate the full range of anticipated targets.

**References are listed at the end of the paper.*

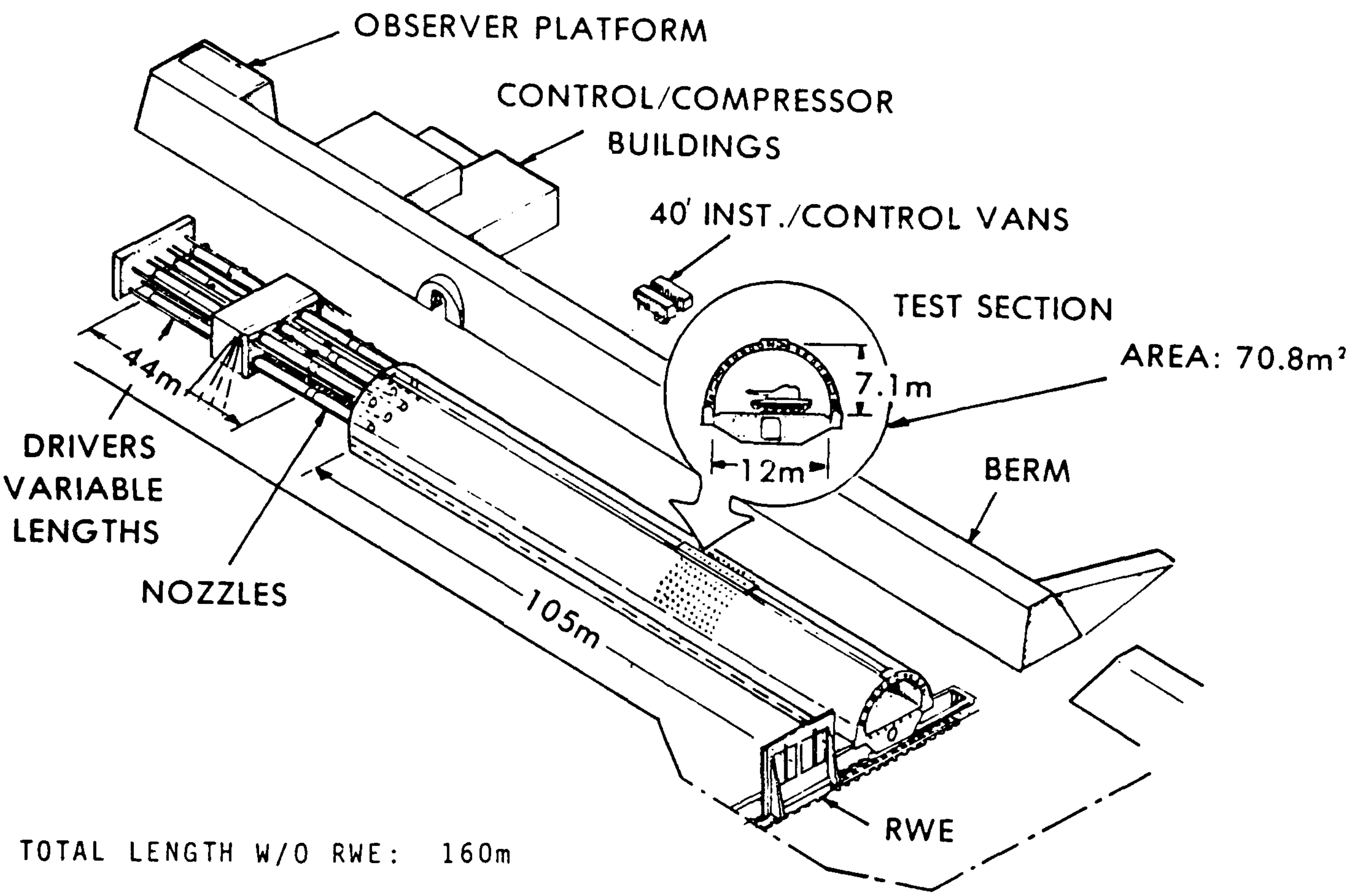

Figure 1. The LBS at the CEG, France

Both a numerical and an experimental approach were chosen but the experimental approach required a longer lead time for building a model facility, while the numerical approach could be realized almost immediately and was more suitable to the quick production of a large number of data points. Numerical methods for solving the Euler equations already existed and an implicit, factored finite-difference scheme was chosen to develop the quasi-one-dimensional BRL-Q1D code[5] for simulating the flow in blast-wave simulators. The experimental effort required much more preparation time for building a model facility that delivered relatively few data points at a later time. The results of the experimental work have been used to validate the computational and analytic work.[6-8]

2. THE U.S. LB/TS CONCEPT

In an LB/TS, blast waves are simulated by releasing compressed gas from several high-pressure steel driver tubes into a large expansion tunnel. Straight shock tubes cannot be used because they do not produce the static and dynamic pressure decay rates which are observed in free-field blast waves. To obtain long flow durations comparable to those of decaying blast waves, the outflow of the driver gas has to be retarded. This is effected by converging the flow area at the exit of the driver so that the latter takes the shape of a bottle. Furthermore, a single driver is technically impractical because the required supply pressures would necessitate an inordinate wall thickness of the driver for the projected size of the LB/TS facility. The size of the diaphragm is limited by steel supplies, also. For these reasons, a number of smaller driver tubes has to be employed to accomodate the necessary initial driver conditions.

2.1 THE LAYOUT OF THE FACILITY

A schematic layout of the advanced concept U.S. LB/TS facility is shown in Figure 2. The shock wave in the expansion tunnel will be driven by an array of nine steel driver tubes [1]. A large concrete reaction pier [2] will anchor the driver tubes in the ground. Each driver tube will measure 1.83 metres (72 inches) internal diameter (ID), will be an average of 80 metres long and composed of up to 10 sections which will either be welded together or connected by flanges to facilitate changes in length. The driver gas will be stored in tanks as liquid nitrogen (LN2) [15]. When the drivers are to be filled, the LN2 will be pumped [16] through nine pebble bed heaters [17] in which it is evaporated and superheated. The gas temperature in the drivers will be controlled by mixing the superheated nitrogen with bypassed liquid nitrogen in a secondary, small pebble bed mixer before it enters the drivers. The inside of the driver walls may or may not be insulated against heat loss by layers of fiberglass embedded in a high temperature resistant polymeric resin depending on the fill rates realized with the pebble-bed heaters.

Convergent nozzles [3] connect the driver tubes with the 0.914 metres ID (36 inch) throat sections. Throat valves and/or diaphragms [4] are mounted in the throat at the

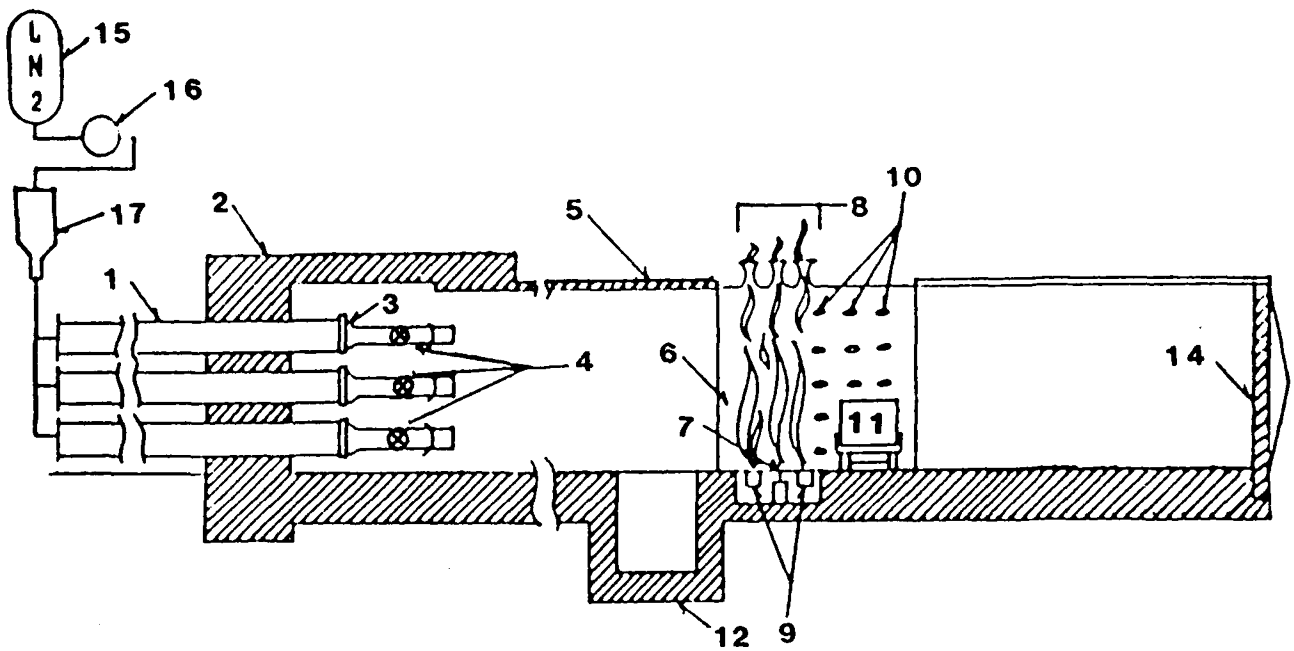

LEGEND

1 - Steel Driver Tubes
2 - Concrete Reaction Pier
3 - Converging Nozzles
4 - Throat Valves and Diaphragms
5 - Concrete Expansion Tunnel
6 - Steel Test Section
7 - Thermal Radiation Sources
8 - Combustion Products Ejectors
9 - Air Curtain Plenum
10 - Instrumentation and Light Ports
11 - Test Target
12 - Soil Tank
14 - Rarefaction Wave Eliminator
15 - Liquid Nitrogen Storage
16 - Cryogenic Pumps
17 - Pebble-Bed Superheaters

Figure 2. The Advanced U.S. LB/TS Concept

exit of the convergent nozzle (the bottle neck). Fast opening and closing valves are the preferred flow control devices over diaphragms because they eliminate the need to adjust the length of the driver tubes for simulating various desired yields. They also eliminate the need to replace the diaphragms before each test. The changing of the driver lengths and of the diaphragms would require a great amount of labor. On the other hand, diaphragms may be needed because fast opening throat valves are not state of the art, and it is presently not known if they will perform in the expected manner. If diaphragms have to be used, a double diaphragm system would have to be employed because the cutting charges which are used to initiate the rupturing of the diaphragms cannot be exposed to heat for safety reasons.

The current design projects an expansion tunnel [5] of semicircular cross-section with a reference area of 165 m^2. The expansion tunnel will be 190 m long and formed of prestressed concrete. A steel test section [6] will be located in the expansion tunnel 100 m downstream from the throat-nozzle exit. The walls of the test section will be equipped with a large number of ports [10] for cameras, lighting and instrumentation. A soil tank [12] for testing shallow buried structures will be located in the floor of the test section. The thermal loading that is associated with blast waves resulting from nuclear explosions will be simulated by thermal radiation sources (TRS) [7], mounted in the floor of the test section just ahead of the target area. The thermal pulse is simulated by aluminum/oxygen combustion. Air curtains fed through nozzles from a plenum in the floor [9] will be placed to both sides of the TRS nozzles to contain the flames and the combustion products. A large number of jet pump ejectors [8] would be mounted in the top of the test section to remove the TRS combustion products from the simulator. A rarefaction wave eliminator (RWE) [14], controlling the flow of gas exiting the expansion tunnel will be located at the end of the expansion tunnel.

2.2 THE LB/TS OPERATING SEQUENCE

The operation of the U.S. LB/TS includes several phases, such as the instrumentation of the target and its placement in the test section, the calibrating of the recording instrumentation in the data acquisition center, the programming of the throat valves and of the RWE, the installation of diaphragms and cutting charges, the preparation of the TRS units, the heating of the driver gas, and the pressurization of the drivers. After final safety checks are performed, the firing sequence is initiated.

In a combined thermal/blast simulation, the thermal pulse will be simulated first. Aluminum and oxygen will be mixed in the TRS nozzles and ignited. The hot aluminum oxide produced by the combustion irradiates the target, producing the thermal simulation. The aluminum oxide is confined and entrained by the air curtains. Natural convection and air curtain entrainment move the aluminum oxide upwards toward the ceiling of the test section, where it is sucked out by the ejector pumps.

After the ejectors have removed the aluminum oxide, the blast wave is initiated either by breaking the diaphragms or by very rapidly opening the throat valves. The shock then forms, moves down the expansion tunnel and begins the blast loading of the target. After the shock is initiated, the throat valves would be closed at a preprogrammed rate to meter the flow, sending forward rarefaction waves which cause the static pressure behind the shock to decay in the same manner as in a free field blast wave. If throat valves were not available, the drivers would be staggered in length so that the rarefaction waves reflected from the nine driver ends at different times would cause the pressure behind the shock to decay.

At the end of the expansion tunnel the flow interacts with the RWE. The RWE partially reflects the primary shock from its vanes and generates rarefaction waves from its open areas which interact with the reflected shocks to cancel each other. The RWE then closes in such a manner that this interaction continues and its exit pressure continually matches the ambient pressure. When the RWE is properly set, neither a rarefaction nor a compression wave will move upstream into the test section. Finally, rarefaction waves generated in the drivers move through the test section, lowering the pressure and decelerating the flow. The simulation ends when the ambient conditions are restored.

2.3 THE OPERATING ENVELOPE

The purpose of the proposed LB/TS is to simulate decaying blast waves similar to those which are generated by nuclear explosions [9] The scope of operating conditions which the LB/TS is expected to emulate is defined by the operating envelopes shown in Figure 3. Two evelopes were chosen for representation, one based on the positive phase duration (Figure 3a), the other one based on the dynamic pressure impulse (Figure 3b). Each blast wave in these envelopes is defined by one shock overpressure (p_{so}) and one positive phase duration (PPD) or dynamic pressure impulse (I_q). The yields represented by these sets of shock overpressures versus PPDs and impulses, respectively, range from 1 to 600 kT for a tactical nuclear air burst with a scaled height of burst of $61 m \times W^{1/3}$, i.e., the height is equal to 61 metres times the weapon yield in kilotons to the 1/3 power.

Figure 3a presents the traditional operational envelope for static overpressure versus PPD which can be related to the diffraction loading of targets. The shock overpressures range from 13.8 to 241.3 kPa and the PPDs from 0.15 to 4.30 seconds. Figure 3b presents the operational envelope for static overpressure versus dynamic pressure impulse. The dynamic pressure impulse is related to the drag loading which is reponsible for the overturning of targets. The impulse values range from .08 kPa-s to 43.11 kPa-s. This envelope clearly indicates the increasing importance of the dynamic pressure impulse at shock overpressures above 50 kPa.

For each of the blast waves defined in the operational envelopes, there exist corresponding initial driver conditions for the LB/TS, such as pressure, volume and temperature . The shape of the decaying blast wave depends either on the driver geometry, or on closing and opening functions for the fast-acting throat valves. Computational simulations were performed with the BRL-Q1D hydrocode to determine these parameters.

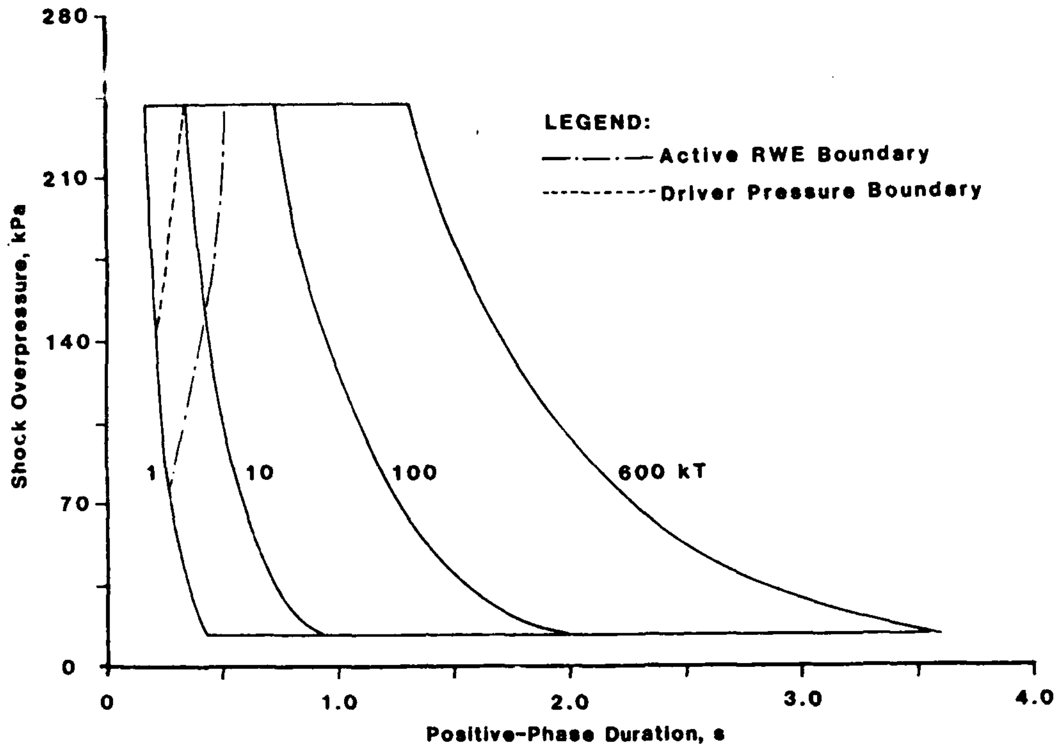

a) based on Positive Phase duration

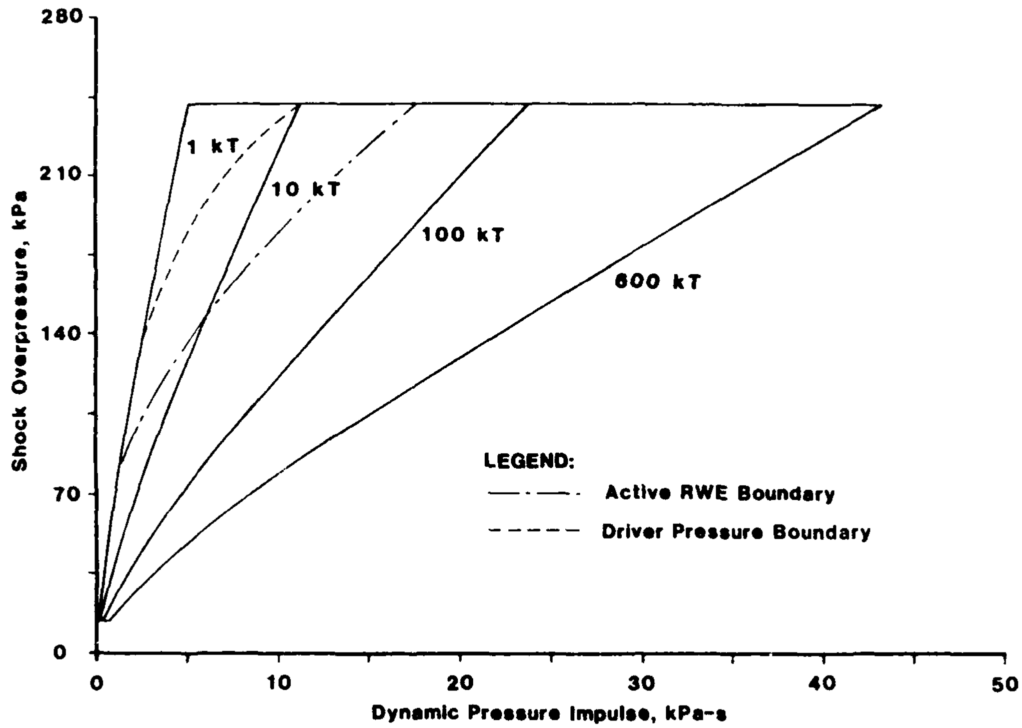

b) based on Dynamic Pressure Impulse

Figure 3. LB/TS Operating Envelope (Source: USA-HDL)

3. THE CFD DESIGN TOOL

The BRL-Q1D code[5] is a computer program written in the FORTRAN 77 language. The code makes the simplifying assumptions that the compressible and time-dependent flow in the LB/TS is quasi-one-dimensional, adiabatic, and inviscid resulting in the one-dimensional Euler equations. The theory, code structure, input requirements and output options of the BRL-Q1D code are described in detail in Reference 5. Here, a synopsis is given for the orientation of the reader.

3.1 THE GOVERNING EQUATIONS

The differential Euler equations which describe the one-dimensional flow are derived for arbitrary geometries in their conservative form. The physical, independent variables, x and t, are transformed into a uniformly-spaced computational grid by a general transformation of the form $\xi = f(x,t)$, and $\tau = t - t_0$. The resulting transformed set of the one-dimensional Euler equations can be written as

$$\frac{\partial \vec{Q}}{\partial \tau} + \frac{\partial \vec{E}}{\partial \xi} + \vec{h} = 0 , \qquad [3\text{-}1]$$

where the transformed vectors are defined as follows.

$$\vec{Q} = \vec{q}\,\tilde{A} = \begin{bmatrix} \rho\,\tilde{A} \\ \rho u\,\tilde{A} \\ e\,\tilde{A} \end{bmatrix} , \quad \vec{E} = \vec{q}\,\tilde{A}\xi_t + \vec{\mathrm{E}}\,\tilde{A}\xi_x = \begin{bmatrix} \rho\,\tilde{A}\xi_t + \rho u\,\tilde{A}\xi_x \\ \rho u\,\tilde{A}\xi_t + (\rho u^2 + p)\,\tilde{A}\xi_x \\ e\,\tilde{A}\xi_t + u\,(e + p)\,\tilde{A}\xi_x \end{bmatrix} , \quad \vec{h} = \begin{bmatrix} 0 \\ -p\dfrac{\partial A}{\partial \xi} \\ 0 \end{bmatrix} ,$$

where subscripts x and t imply partial differentiation and $\tilde{A} = A/\xi_x$. This set of three scalar equations represents the conservation of mass, momentum, and energy, per unit volume, with the usual notation of ρ as density, u as velocity, e as total energy per unit volume (!), and p as pressure. The cross-sectional area, A, may vary with the linear dimension, ξ and/or with time, τ. The system of Equations [3-1], together with the ideal-gas equation of state

$$p = (\gamma - 1) \cdot (e - \frac{\rho}{2}u^2) , \qquad [3\text{-}2]$$

where γ is the ratio of specific heats, constitutes the governing set of one-dimensional Euler equations with arbitrary geometry.

3.2 THE IMPLICIT NUMERICAL SCHEME

These equations are numerically applied to the variable-area shock-tube problem using the implicit "Delta" formation of Beam and Warming.[10] Implicit time differencing and central spacial differencing are employed to evaluate the derivative terms in Equation [3-1] while the source term, $\vec{h}$, is evaluated explicitly. Beam and Warming have shown[11] that the system of equations can be solved by one iterative step when the nonlinear terms contained in the vector $\vec{E}$ are locally linearized. To control phase errors associated with the highest frequencies, a fourth-order dissipation term is explicitly added to Equation [3-1] in its difference form. The final form of the computational algorithm which has been programmed becomes then

$$\left[\mathbf{I} + \Delta\tau\delta_\xi \, \mathbf{A} \right]_j^n \cdot (\Delta \vec{Q})_j = - \Delta\tau\delta_\xi \, (\vec{E})_j^n - \Delta\tau \, (\vec{h})_j^n + \epsilon \, (\Delta_\xi\nabla_\xi)^2 \, \vec{Q}_j^n \, , \qquad [3\text{-}3]$$

where δ_ξ indicates central spacial differencing, $\mathbf{I}$ is the identity matrix and $\mathbf{A}$ is the Jacobian of the convective terms with respect to the flow variables, $\partial\vec{E}/\partial\vec{Q}$. In the actual implementation of Equation [3-3], the left-hand term in brackets is a tridiagonal system which is solved by matrix inversion.

At the endpoints of the grid, appropriate boundary conditions were defined. The reflective boundary at the left-hand side of the grid (i.e., the closed end of the driver) was computationally modeled by means of image points, such that $\rho_1 = \rho_3$, $u_1 = -u_3$, $u_2 = 0$, and $e_1 = e_3$. At the right-hand side of the grid (at the open end of the expansion tube) boundary conditions for outflow as well as for inflow were defined. For outflow, the static pressure is specified and for inflow, the density is specified, additionally. The remaining flow variables are then computed from one-sided differences at the exit plane using backward differencing in space and forward differencing in time.

3.3 IDEAL BLAST WAVE REFERENCE

At the end of the computation, the blast-wave history is compared to an ideal blast wave in order to classify the computational results. A tabulation of a 40 kT free field blast wave for a height of burst (HoB) of 208.5 m (i.e., $61\,\mathrm{m/kT^{1/3}}$ HoB) is used as the reference data base for generating ideal blast wave histories of various overpressures and yields. A computational blast wave is said to approximate an ideal blast wave if the peak overpressure, the positive phase duration and the impulse correspond to the free field parameters associated with the ideal blast wave. The pressure history of an ideal blast wave is defined in Figure 4.

The static overpressure history $p(t)$ of an ideal blast wave can be described conveniently by the modified Friedlander equation.[9] This equation describes the pressure history in terms of three parameters, i.e., the primary shock overpressure p_{so}, the positive phase duration T_+ and the pressure decay constant β.

$$p(t) = p_{so} \left(1 - \frac{t - t_a}{T_+} \right) e^{-\beta \frac{t - t_a}{T_+}} , \qquad [3\text{-}4]$$

where $$t_a < t \leq t_a + T_+ \, . \qquad [3\text{-}5]$$

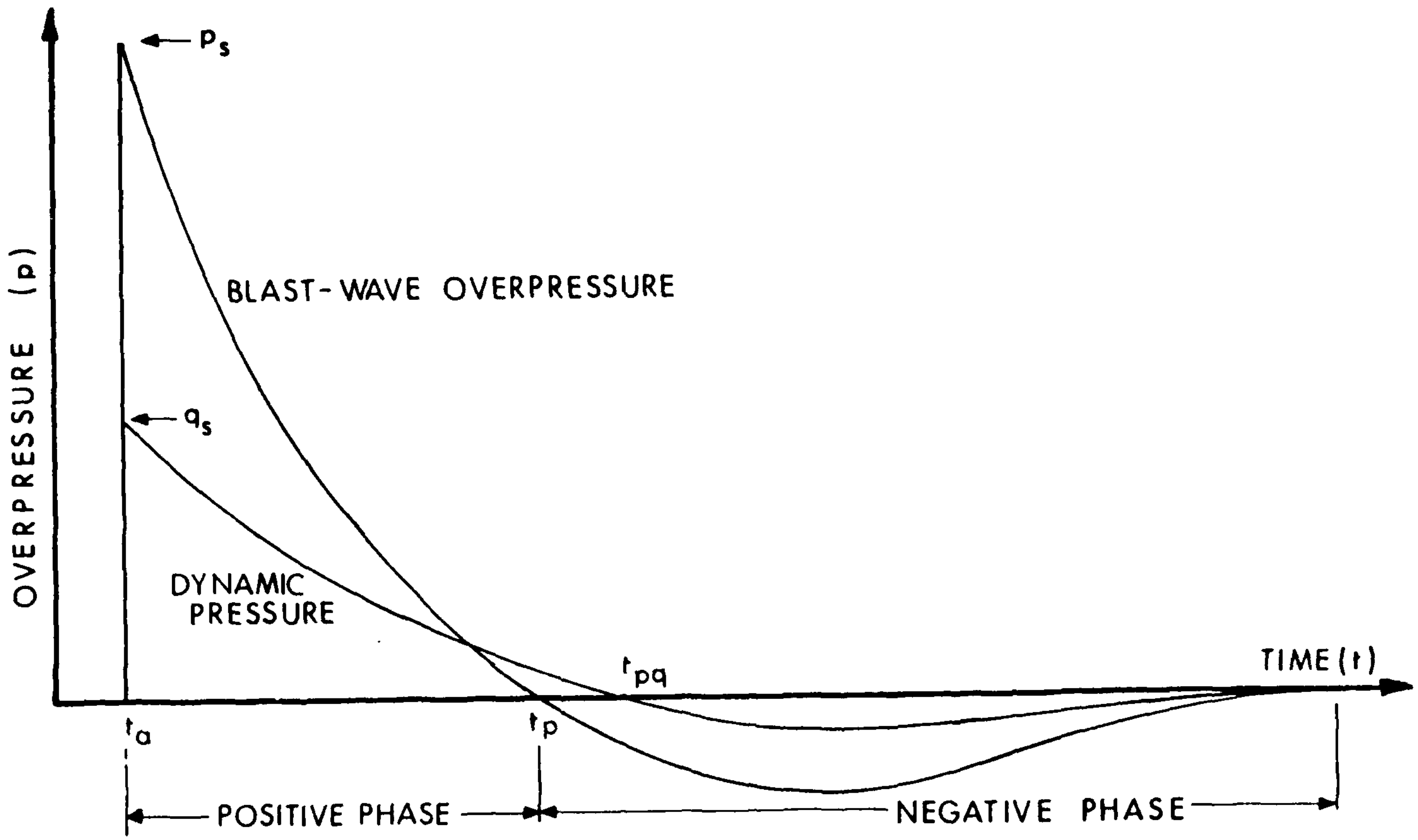

Figure 4. Ideal Blast Wave Definition

The side-on overpressure impulse of the positive phase is defined by the integral in time of the overpressure over the positive phase.

$$I_s = \int_{t_a}^{t_a+T_+} p(t)\,dt. \qquad [3\text{-}6]$$

The decay constant β may be obtained from the integrated impulse equation when the overpressure impulse is known.

The shock front of the blast wave passing through the air not only increases the static pressure, but also the density ρ and the temperature Θ, and accelerates the air in the direction of its travel producing the flow which generates the dynamic pressure. The dynamic-pressure history $q(t)$ and the dynamic-pressure impulse I_q are described by analogous equations with the exception that the parameters are now the peak dynamic pressure q_s, the wind positive-phase duration T_{+q} and the dynamic-pressure-decay constant β_q. Both decay constants were determined from the appropriate static and dynamic pressure impulses and included in the data base.

4. COMPUTATIONAL DESIGN STUDIES

In this section, the results of parametric design studies are reported which were carried out at the BRL to characterize the proposed U.S. LB/TS facility and to determine the influence of specific components or features on the technical performance of the facility. First, the facility was characterized based on the design of the CEG LBS. Conclusions drawn from that study led to the investigations of driver gas heating[12] and the use driver baffles[13] or throat valves instead of diaphragms[14,15] for wave shaping.

4.1 THE COMPUTATIONAL U.S. LB/TS MODEL

The U.S. LB/TS is modeled for the BRL-Q1D code in the same fashion in which the CEG LBS was modeled previously.[3] In order to simulate the U.S. LB/TS in a quasi-one-dimensional context, the total cross-sectional area at any lengthwise location has to be determined by lumping the individual driver and nozzle areas together into one. The present U.S. LB/TS concept differs from the French concept in the number and size of the drivers and in the use of heated driver gas. Furthermore, the cross-sectional reference area of the U.S. LB/TS is more than twice that of the CEG LBS. However, the area ratios between the driver, nozzle throat, and expansion tunnel are the same as in the CEG LBS. The reference data of the U.S. LB/TS are listed in the following Table.

The computational model of the U.S. LB/TS is shown in Figure 5. The nine drivers of the proposed U.S. LB/TS (Figure 5a) are combined into one in the same

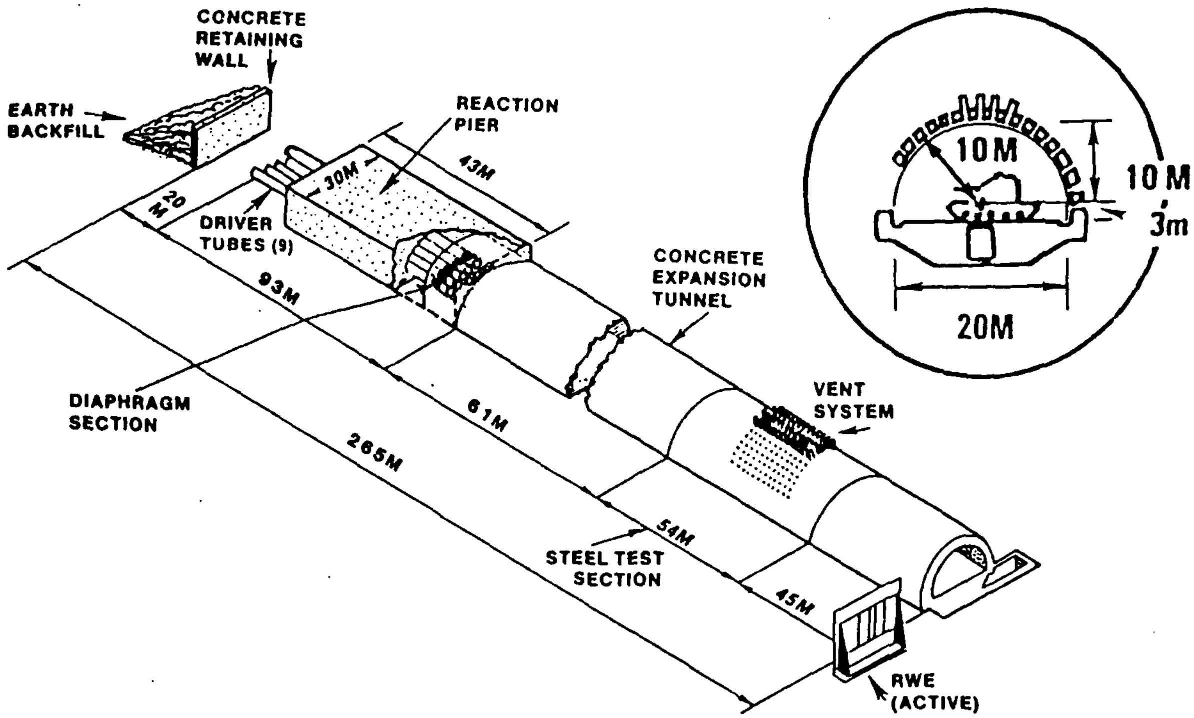

a) The Proposed U.S. LB/TS Facility

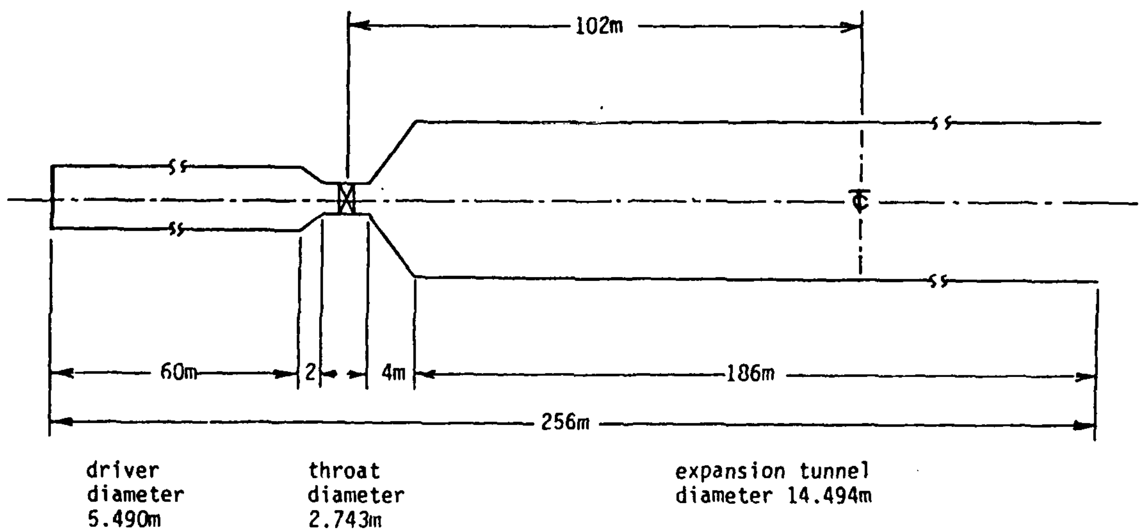

b) The Quasi-One-Dimensional Model

Figure 5: The Computational LB/TS Model

U.S. LB/TS REFERENCE DATA	
DRIVERS	
Reference Volume (9 drivers), V_{ref}	1450 m^3
Reference Length, L_{ref}	60.0 m
Nominal Diameter, D_{drv}	1.829 m
Ratio of Throat-to-Driver Area	1:4
EXPANSION TUBE	
Reference Area, A_{ref}	165 m^2
Reference Hydraulic Diameter (RHD), D_{ref}	14.494 m
Test Section Location Measured from Nozzle Exit, X_{sta}	101.5 m
Nominal Expansion-Tunnel Length, L_{net}	191 m
Ratio of Throat-to-Reference Area	1:28

manner as was done with the CEG LBS. A single cylindrical driver representing the nine drivers of equal length (Figure 5b) was modeled for the computations of valve closing functions, in which the shaping of the blast wave was simulated by the use of a fast-acting throat valve. The fast-acting valve in the throat of the nozzle was modeled as a parabolic constriction with time-dependent cross-sectional area. The cylindrical driver shape was also used for determining the driver gas heating for matching the density across the contact surface. The U.S. LB/TS concept does not utilize divergent nozzles at the present time; but they will be included if future tests in the prototype facility reveal large flow losses. However, a divergent nozzle had to be retained in the computational model to facilitate the expansion of the computational flow.

4.2 DRIVER GAS HEATING

The complex flow patterns encountered in an LB/TS were described in detail in Reference 3 for an LB/TS operated with cold driver gas. Generally, the flow in an LB/TS is distinguished from the flow in a conventional shock tube by the occurrence of choked flow in the throat of the nozzle, and a recompression shock compensating for the supersonic expansion of the flow exiting the choked throat of the nozzle (Figure 6). For high shock overpressures, the recompression shock (10) is swept out of the nozzle and down the expansion tube. It is followed by a region of supersonic flow (9) at extremely low static and high dynamic pressure. At later times, the recompression shock returns to the nozzle exit where it is partially reflected (15) and partially transmitted, moving upstream into the drivers. The parametric design studies with unheated driver gas have also shown that the density across the contact surface (3) between the gas originally in the driver and the shocked gas originally in the expansion tunnel is severely mismatched for shock overpressures above 100 kPa. The high dynamic pressure due the density difference across the contact surface also does not properly simulate a free-field, exponentially decaying blast wave.

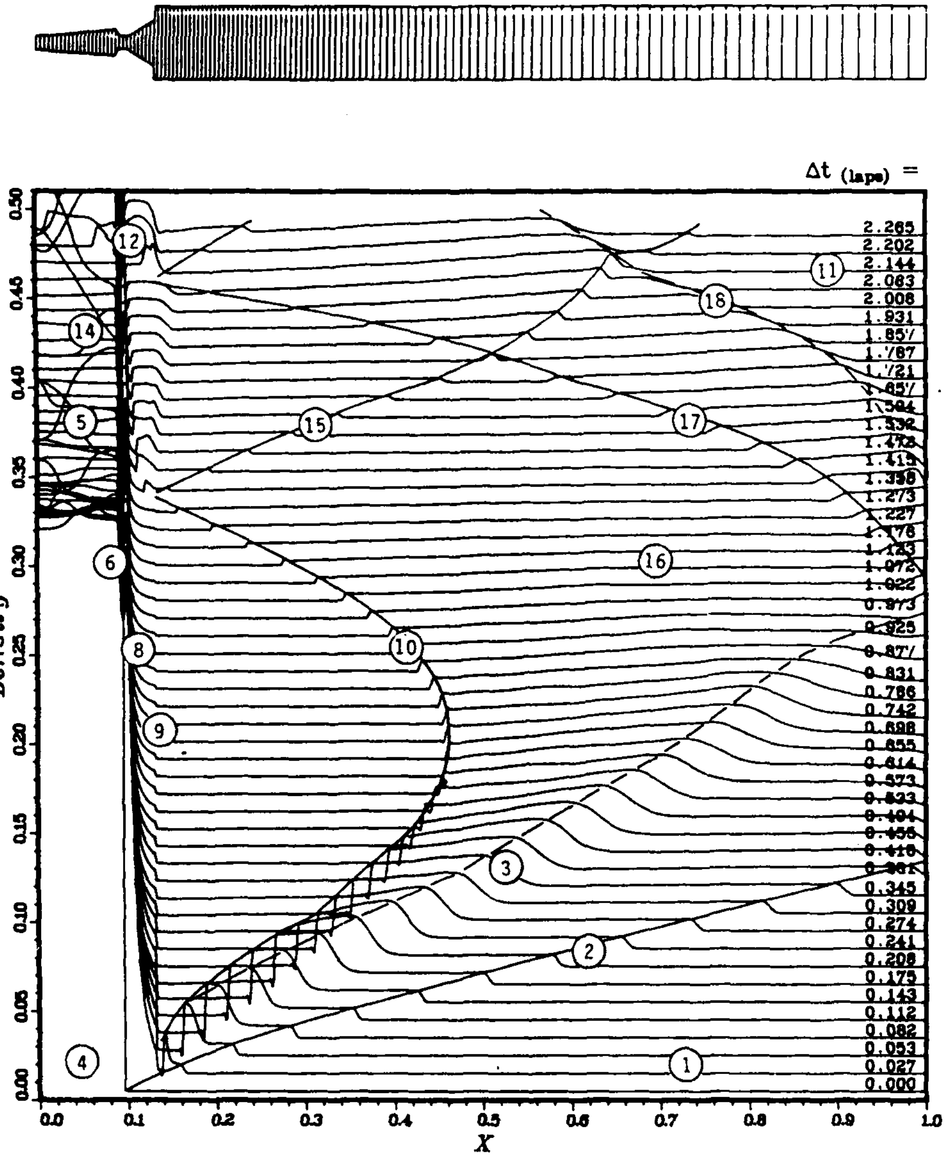

LEGEND

EARLY-TIME FLOW PATTERN		LATE-TIME FLOW PATTERN	
1	Ambient Conditions	11	Inflow at Ambient Pressure
2	Principal Shock	12	Isentropic Compression of Subsonic Flow
3	Contact Surface	14	Rarefaction Wave Reflected from Driver End
4	Initial Driver Conditions	15	Recompression Shock Partially Reflected from Nozzle Exit
5	Rarefaction Wave	16	Rarefaction Wave Transmitted through Nozzle
6	Isentropic Expansion of Subsonic Flow and Choked Flow in Throat	17	Recompression Wave from Open End of Expansion Tube
8	Isentropic Expansion of Supersonic Flow	18	Contact Surface from Open End of Expansion Tube
9	Density Discontinuity at Nozzle Exit		
10	Recompression Shock		

Figure 6. Illustration of Physical Flow Phenomena.

The computations for unheated driver gas indicate that in extreme cases, the recompression shock may be swept past the test station, destroying the blast wave simulation in the process (Figure 7a). The recompression shock can be avoided by relocating the test section a few diameters downstream (Figure 7b), but it is not possible to avoid the contact surface which, under many high-yield conditions in the Q1D analysis, can arrive at the exit of the expansion tunnel (Figure 6). The high dynamic pressure which follows the contact surface severely distorts the shape of the dynamic pressure history (Figure 7b) on which the overturning criteria for military equipment are based. For these reasons, heating of the driver gas is considered imperative for the successful operation of the U.S. LB/TS at higher shock overpressures.

Following a parametric study of the shock overpressure versus driver pressure[9] it was discovered that an LB/TS using cold driver gas would require extremely thick driver walls (in excess of 30 cm) because of the necessary high driver pressures. Appropriate heating of the driver gas will (a) reduce the maximum required driver pressure and thereby reduce the thickness of the driver walls and the cost of the drivers; (b) eliminate the density discontinuity across the contact surface thus properly representing the dynamic pressure history of the simulated blast wave; and (c) weaken the recompression shock of the overexpanded driver gas because the heated gas contains more energy for the expansion in the nozzles. Driver heating does, however, accelerate the decay of the primary shock strength at low-yield simulations because the rarefaction waves in the short drivers catch up to the primary shock faster. This problem can be overcome by providing a secondary test section closer to the nozzle exit and/or the use of throat valves instead of diaphragms.

The severest handicap of operating the planned LB/TS with cold driver gas is the mismatch of the density across the contact surface between the driver gas and the shocked air in the expansion tunnel (Figure 7). By properly heating the driver gas before it is released into the expansion tunnel, the density in the driver gas is lowered such that after expanding in the nozzle and processing through the recompression shock it has the same density as the shock-processed air in the expansion tunnel. In the general notation of the shock tube problem[16], the physical flow regions before and after the contact surface are denoted by the subscripts (2) and (3) and the flow conditions connecting the two regions are $p_2 = p_3$ and $u_2 = u_3$. For matching the density across the contact surface, $\rho_3 = \rho_2$, the initial driver gas temperature has to be adjusted such that after the gas has been expanded in the nozzle and processed through the recompression shock, it's temperature equals the temperature of the shocked air in the expansion tunnel, $T_3 = T_2$.

To determine the proper driver gas temperature T_4 for density matching as a function of the shock overpressure p_{so}, the driver temperature ratio $T_{41} = T_4/T_1$ for an assumed diaphragm pressure ratio $P_{41} = P_4/P_1$ was adjusted until the numerical values in a tabulation of the density history matched before and after the contact surface had passed the test station, seven RHDs downstream from the nozzle throat exit. The subscripts 4 and 1 refer to the initial physical flow regions in the driver (4) and in the expansion tunnel (1). Figure 8 gives an example of matched density across the contact

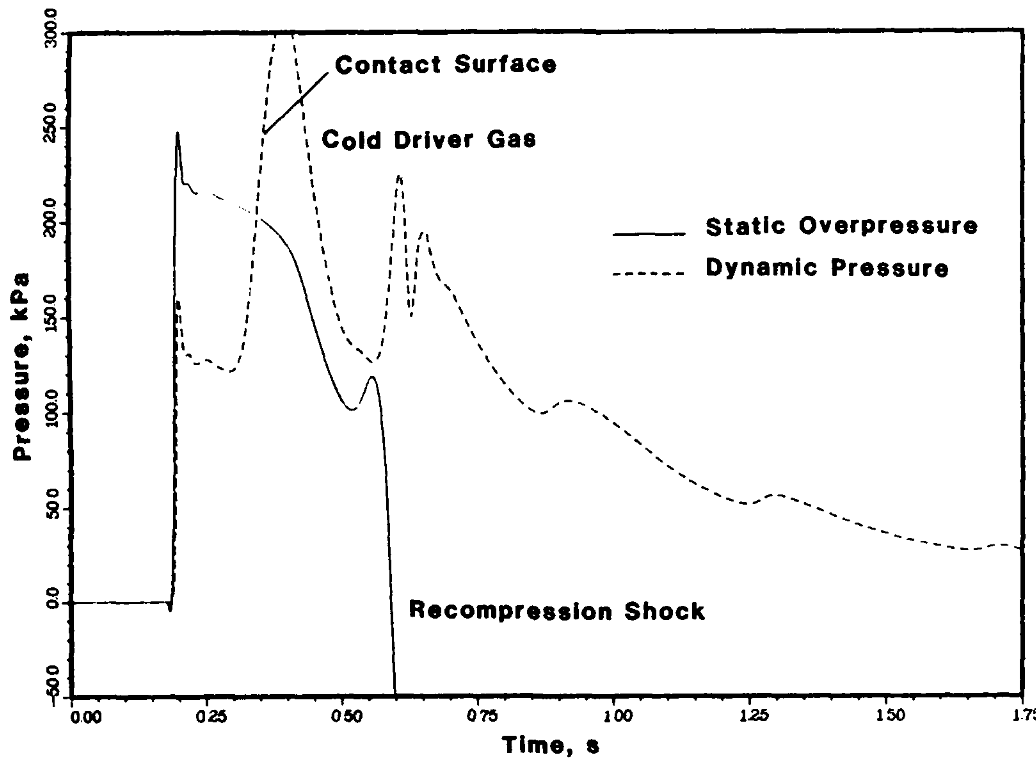

(a) Test Station 7 RHD from the Throat Exit

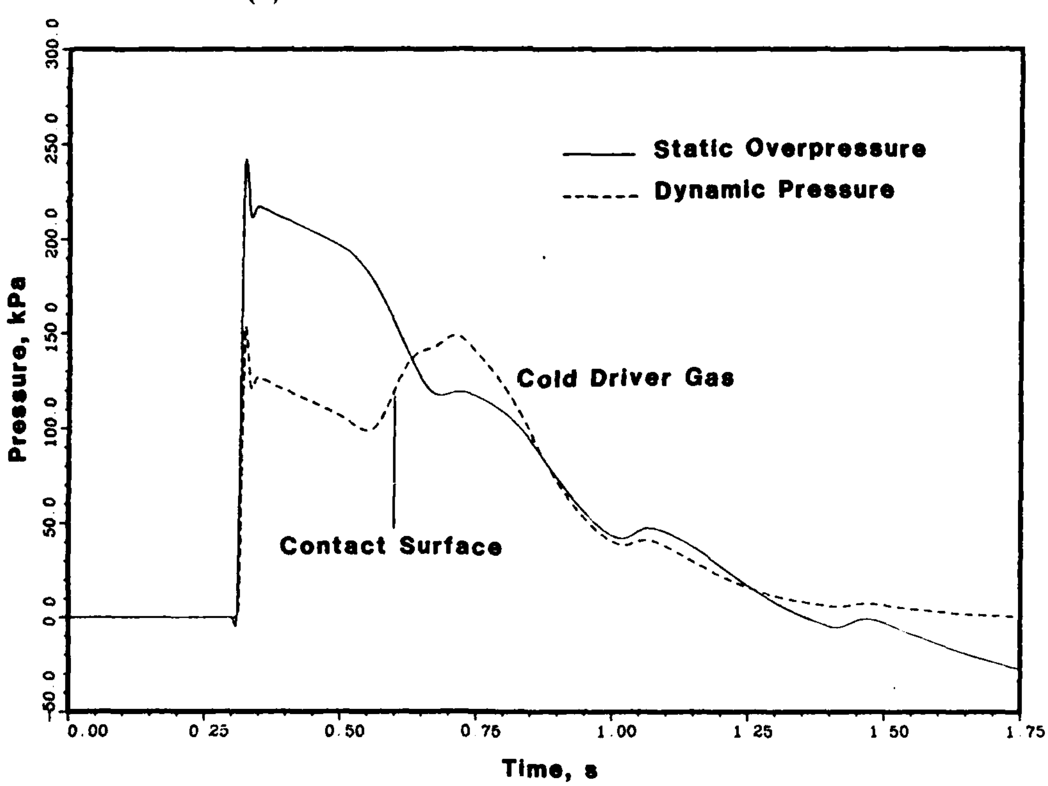

(b) Test Station 12 RHD from the Throat Exit

Figure 7. Recompression Shock and Contact Surface in the Test Station for a 241 kPa & 600 kT Blast Wave

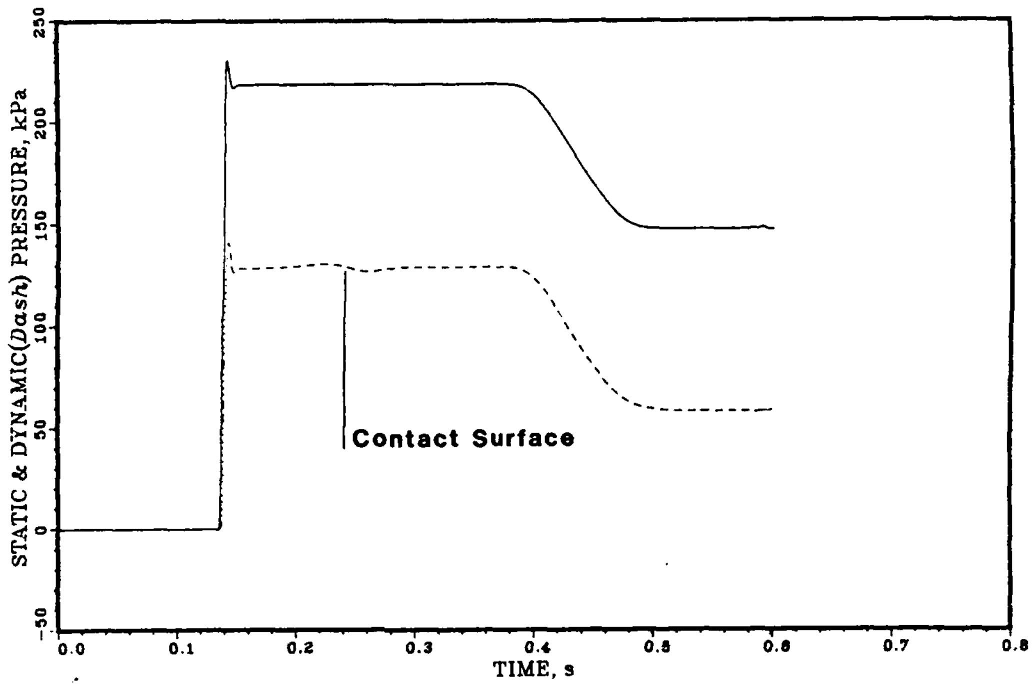

(a) Cylindrical Driver Shape

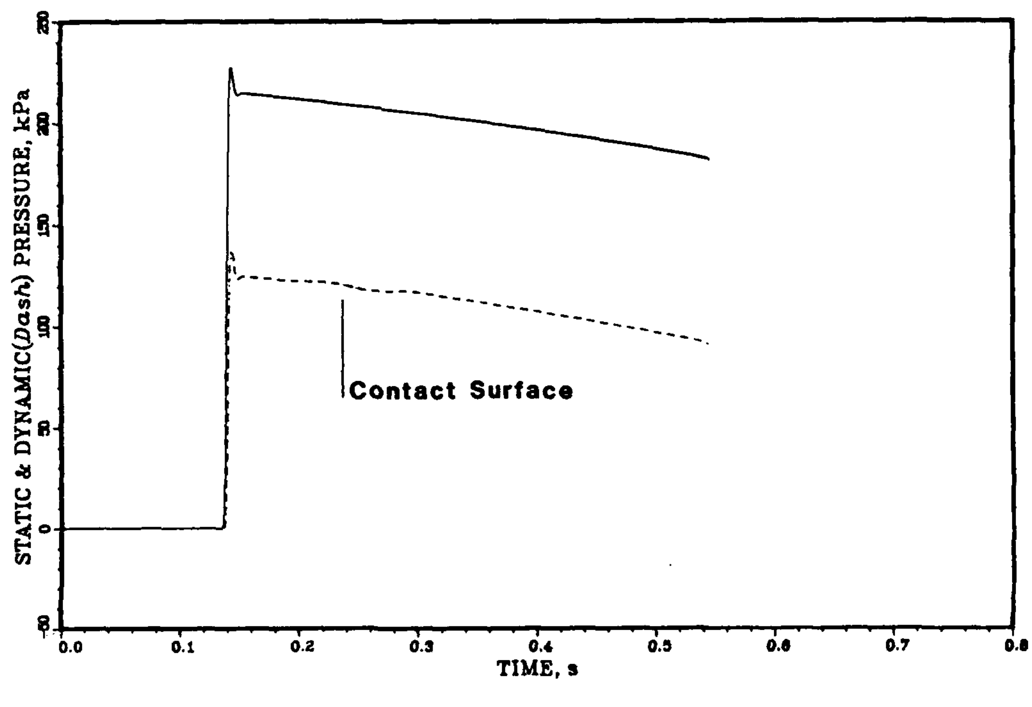

(b) Conical Driver Shape

Figure 8. Matched Contact Surface for a 241 kPa & 600 kT Blast Wave

surface for the case of a 241 kPa shock. The position of the contact surface is not well defined in the computational results. The contact surface is spread out and passes the test station over some time, which can be recognized by the wiggle in the middle of the otherwise smooth dynamic pressure curve.

In Figure 8a, the initial phase of the dynamic pressure history for a long, cylindrical driver is recorded beyond the arrival of the first rarefaction wave from the end of the driver. The wiggle of the dynamic pressure trace in the middle of the upper plateau is due to the gas that was initially in the (computational) convergent-divergent nozzle. The temperature ratio T_{41} for a 241 kPa blast wave is 2.173, which means 626 K (667 °F) based on standard atmospheric temperature at sea level. In Figure 8b, the dynamic pressure history with matched contact surface is shown for a decaying blast wave. The dynamic pressure decays at a noticeably increased rate after the passage of the contact surface (wiggle) and it is therefore difficult to define a matching density for the conical driver in the same manner as was done for the cylindrical driver. However, the difference, if any, appears to be small enough to safely assume that the same initial driver conditions satisfy the criterion of contact surface matching for both drivers.

Computations were carried out for a long cylindrical driver at fourteen diaphragm pressure ratios ranging from 18 to 120 and compared with Pearson's predictions.[12] Since the two data sets agreed well, all data were combined and smoothed by a least-squares approximation using a cubic-spline with variable knots.[17] The resultant functions are presented in Figures 9 and 10. Figure 9 shows the driver-gas temperature ratio T_{41} for which the density across the contact surface is matched, as a function of the shock overpressure p_{s0}. The shock overpressure at the front of the blast wave is the significant parameter which drives the initial conditions in the LB/TS. It is therefore important to relate the initial driver conditions to this significant blast wave parameter.

Figure 10 presents the function of shock overpressure p_{s0} at the test station, seven RHDs (cf. Table on pg. 13) downstream from the throat exit, versus the diaphragm pressure ratio P_{41}. The differences between the two predictions are indicative of the limitations imposed on the Q1D computations by choosing a limited, and different, number of grid points and distributions since both authors followed the same evaluation procedure. Neither prediction can be said to be more accurate than the other one, but the differences are insignificant. The results show that by heating the driver gas, the maximum driver pressure ratio P_{41} for producing a 241 kPa shock at the test station is reduced to 118.7 down from 185.0 for cold driver gas, corresponding to 12.027 MPa (1744 psi) for standard atmospheric pressure at sea level as compared to 18.745 MPa (2719 psi) when the driver gas is cold. It is noted that these values are only theoretical and that the experimental driver pressures will be higher. The tabulated results are enclosed as Appendix A.

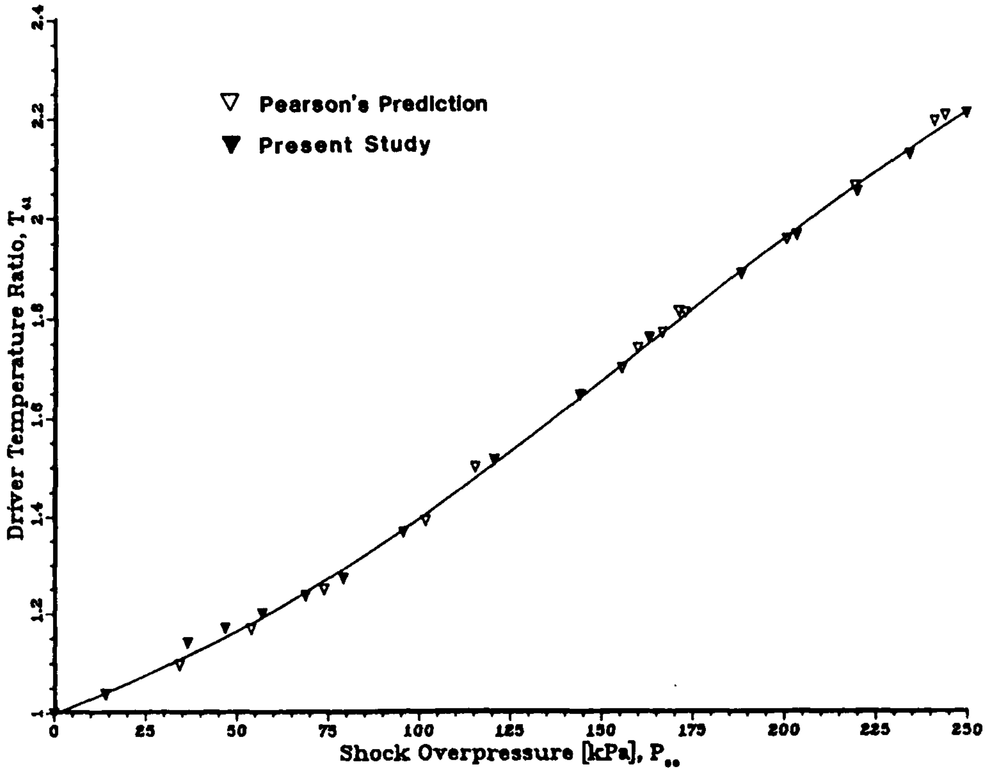

Figure 9. Driver Gas Temperature Ratio Versus Shock Overpressure

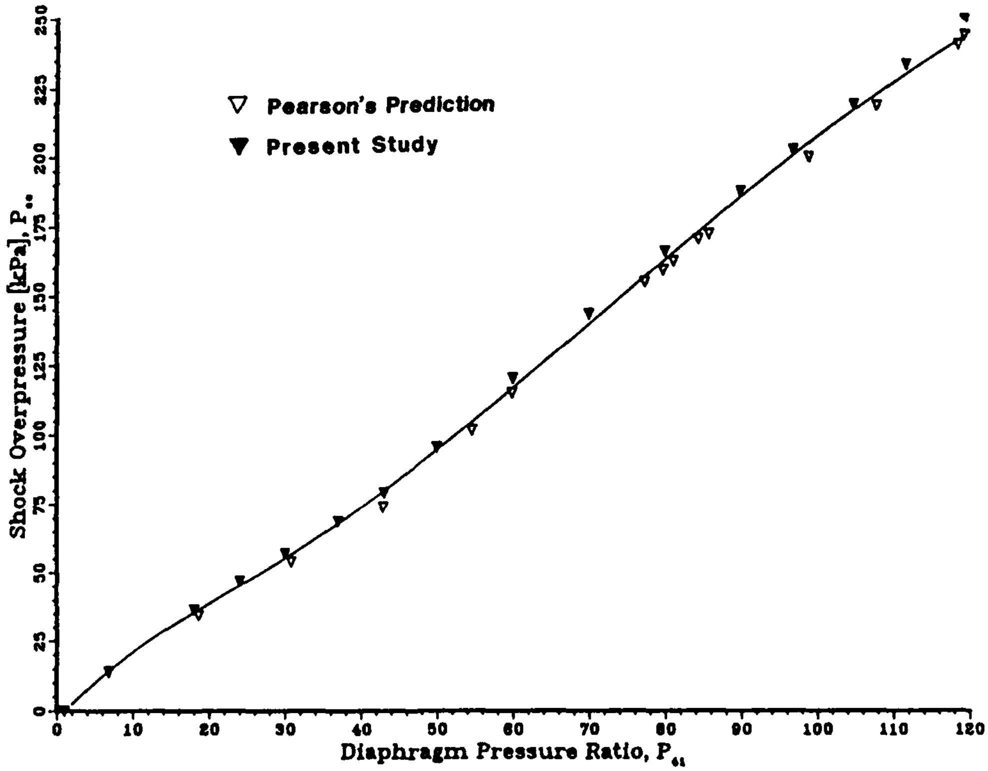

Figure 10. Shock Overpressure at Test Station Versus Driver Pressure Ratio

4.3 THROAT VALVES

The decay of the static and dynamic pressure necessary for the simulation of a blast wave may be produced in a variety of ways. In the absence of special shaping devices like baffles or throat valves, the blast wave is shaped by the rarefaction waves reflected at the closed driver ends. The end walls of the drivers send the reflected rarefaction waves downstream through the nozzles into the expansion tunnel where they overtake the primary shock weakening it in the process. By designing the drivers with various lengths, the rarefaction waves can be made to arrive at different times, giving the blast wave a decaying, although stepped shape. The disadvantage of this method is that the driver lengths would have to be changed for varying the equivalent weapon yield at any given blast-wave overpressure.

Another method for shaping the simulated blast waves would make use of baffles in the driver.[19] However, computational studies by this author have shown that the position of these baffles would have to be adjusted specifically for each overpressure and weapon yield simulated in the LB/TS. The idea was thought to be impractical and therefore abandoned. A third method for blast-wave shaping would employ computer controlled, fast-acting throat valves[15,18] to meter the gas flow out of the drivers.

Fast opening and closing throat valves offer the most elegant method of blast-wave shaping because they are reusable and versatile, and eliminate the need for changing the length of the drivers as well as the diaphragms both of which require a great deal of mechanical labor. Also, diaphragms would be very expensive and difficult to handle because of the high driver pressures and temperatures encountered in the blast-wave simulator. Such fast-acting valves are currently beyond the state of the art, however, and need to be developed. If valves can be developed that open fast enough to initiate the shock at least at high overpressures, this method would produce a significant cost savings in the operation of the LB/TS.

The first function of the throat valves is to initiate the shock by rapidly opening the throat-valve area, thus simulating a rupturing diaphragm. In order for the primary shock to be considered properly formed, its rise time, i.e., the time it takes the blast-wave pressure to rise from 5% to 95% of its maximum, must be under 0.5 ms. The time in which the valve has to open in order to produce a shock rise time of 0.5 ms at the test station was determined computationally[19] for the full range of shock overpressures, i.e., from 13.8 to 241.3 kPa using the BRL-Q1D code. The results of this study are re-presented in Figure 11.

The longest opening time at which the shock is still properly formed according to the above stated criterion was found to be 64 ms for the highest principal shock overpressure of 241 kPa, and 26 ms at the lowest shock overpressure of 13.8 kPa. These requirements were included in the design specifications for a 1:2 scale prototype valve. However, such short opening times may be difficult to achieve and therefore, the present design combines the throat valves with a diaphragm to initiate the shock at low shock overpressures. Most likely, the diaphragm would be located downstream of the valve

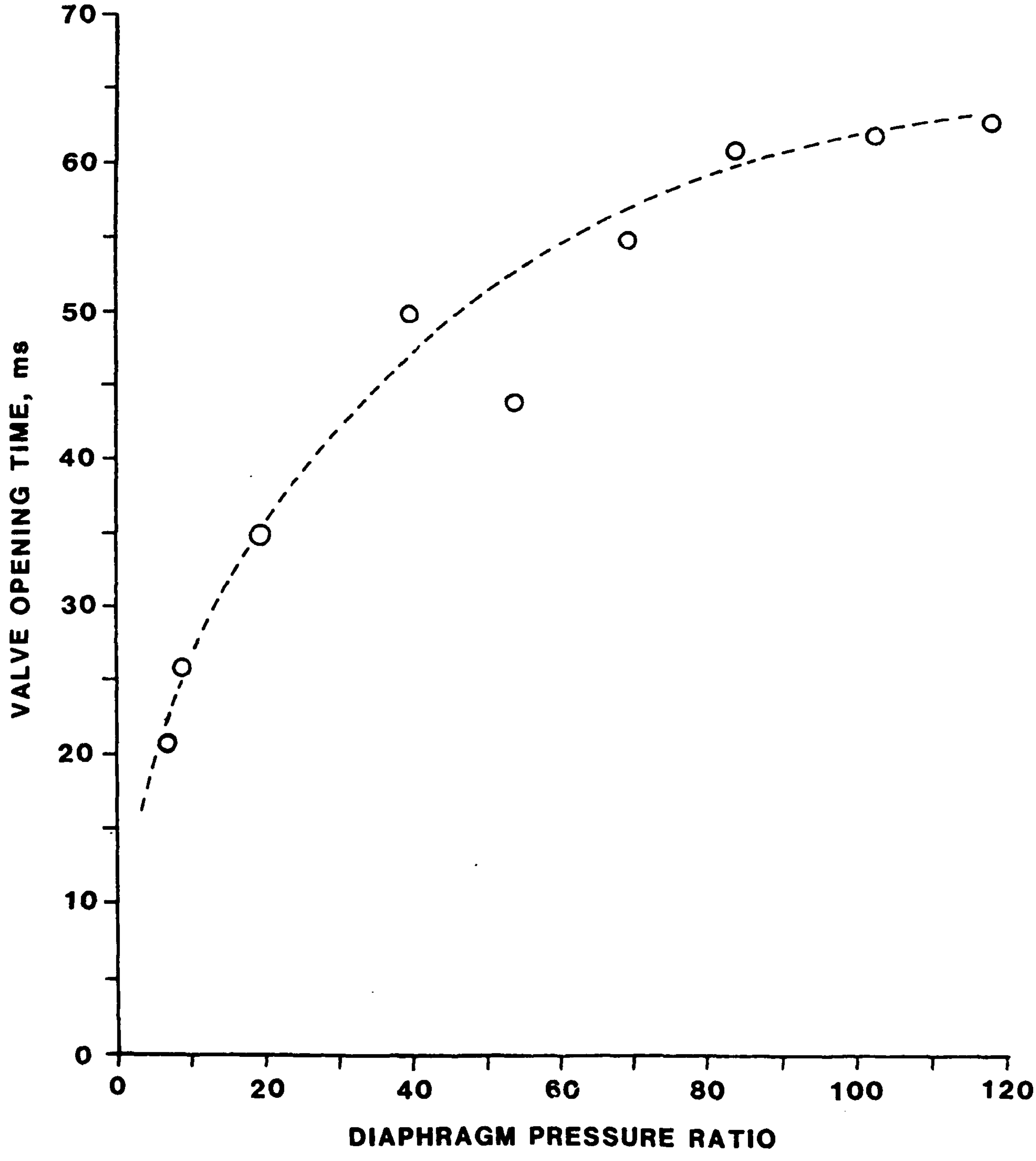

Figure 11. Maximum Allowable Valve Opening Time Versus Diaphragm Pressure Ratio[19]

and opened by cutting charges. A double diaphragm system would not be needed since heating is not required at the low-pressure end of the operating envelope.

The second function of the valve is to shape the decay of the blast wave in the expansion tunnel. The blast wave decay is controlled by closing the valve as a function of time in a predetermined manner after the shock has been initiated. The closing times for the valve should be close to the positive-phase durations of the nuclear blast waves which are simulated. For the range of shock overpressures and yields projected for the LB/TS, the closing times should range from approximately 0.08 to 4.3 seconds. The four closing functions for upper and lower limiting shock overpressures, i.e., 241 and 13.8 kPa, and high and low yields in the operational envelope, i.e., 600 and 1 kT, were determined computationally with the BRL-Q1D code. A delay of 20 to 50 ms between the shock initiation and the start of the valve closing was assumed to insure that the rarefaction waves generated by the closing process will not overtake the principal shock and cause a loss of shock overpressure before the shock reaches the test section.

The modified Friedlander equation (Equation 3-4) was used to obtain the first estimate of the open valve area versus time assuming that the pressure ratio $p(t)/p_{so}$ would be a measure of the open/total area ratio of the valve. The function was digitized and entered with the input data stream into the BRL-Q1D code computation. The resulting pressure and impulse histories were compared with the pressure and impulse histories of the projected ideal blast wave. Corrections were then applied to the input valve-closing function and the computations were repeated until the resulting blast wave matched the ideal curve. The four matching dynamic pressure histories for the simulated blast wave conditions, i.e., 241 kPa & 1 kT, 241 kPa & 600 kT, 13.8 kPa & 1 kT and 13.8 kPa & 600 kT are shown in Figures 12 through 15 together with the valve closing functions which were used to generate them. The valve closing functions are tabulated in Appendix B.

The valve closing functions were included in the design specifications for a 1:2 scale prototype valve. The Idaho National Engineering Laboratory (INEL) was approched with these specifications and contracted to perform a conceptual design study. Five separate conceptual designs were proposed by valve vendors and INEL.[20] Among these, the most promising design was a multi-element, double sliding sleeve type which was chosen for the design and manufacture of a 1:2 scale prototype valve. This valve design employes 19 identical valve elements with the total effective flow area equivalent to the flow area of the nozzle throat. The elements are pneumatically operated to either a fully open, or a fully closed position at a fixed rate less than, or equal to, 10 ms. By closing the element valves sequentially, a stepped closing profile is generated which approximates the specified closing functions. Control for the sequential closing schedule will be provided by a digital computer which will time the closing of each valve element.

For the blast wave initiation, all valve elements will be opened simultaneously, except in the 13.8 kPa case, where only eight valve elements will be opened. The open valve elements will then be closed sequentially in symmetric pairs, except in the 13.8 kPa (2 psi) case and for the one centrally located element. This leaves ten steps

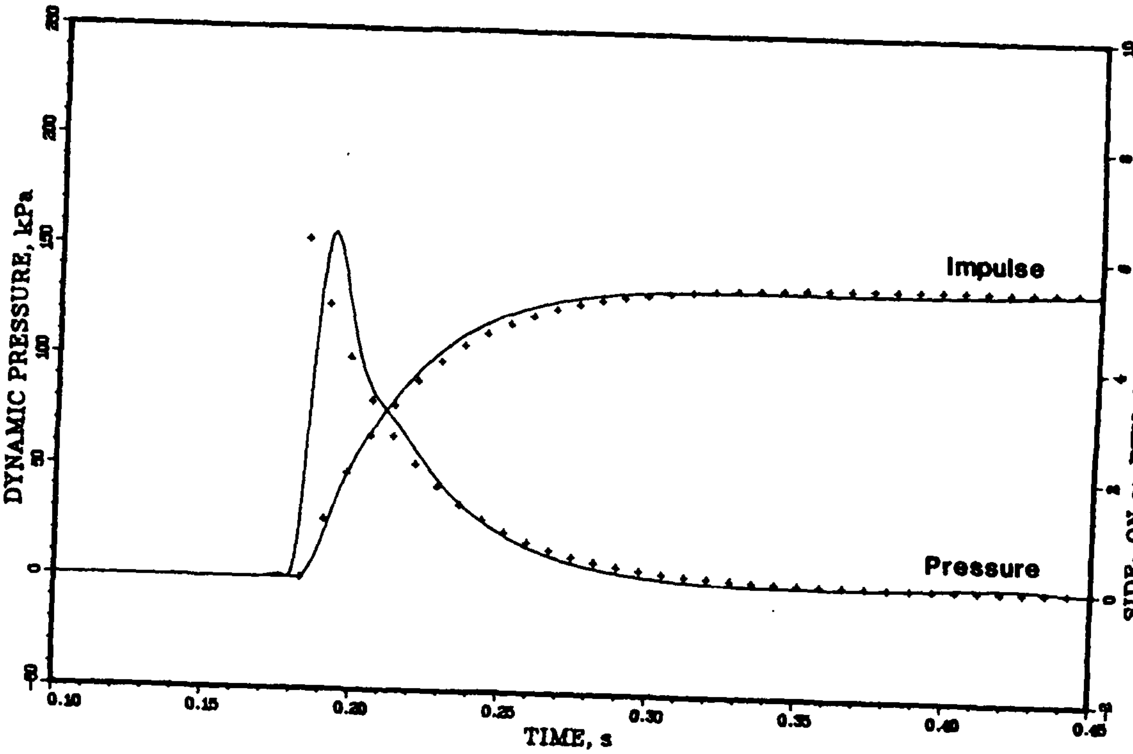

(a) Computed vs Ideal Dynamic Pressure and Impulse Histories

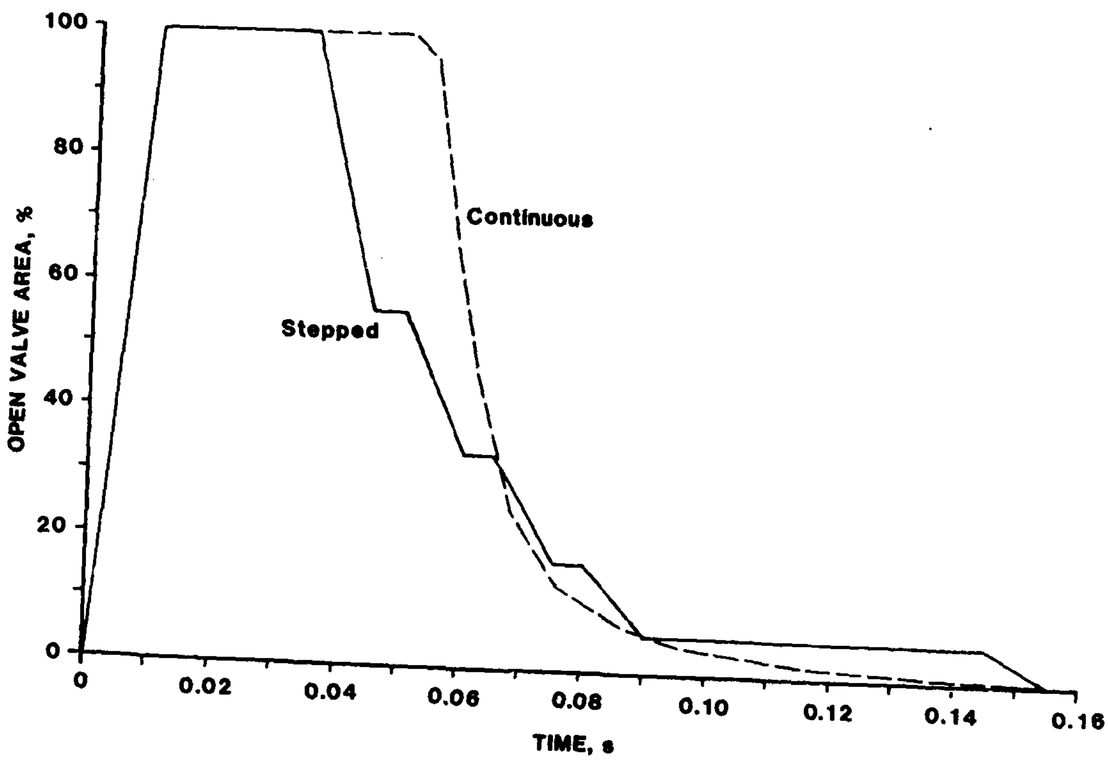

(b) Continuous and Stepped Valve Opening and Closing Functions.

Figure 12. Simulated 241 kPa & 1 kT Blast Wave

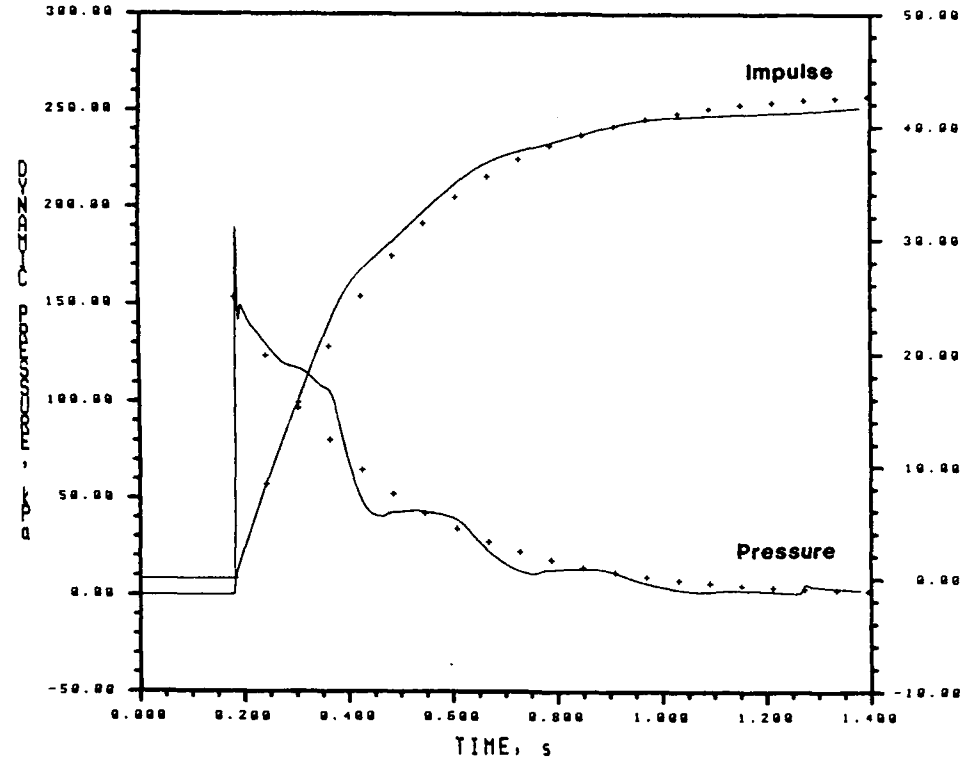

(a) Computed vs Ideal Dynamic Pressure and Impulse Histories

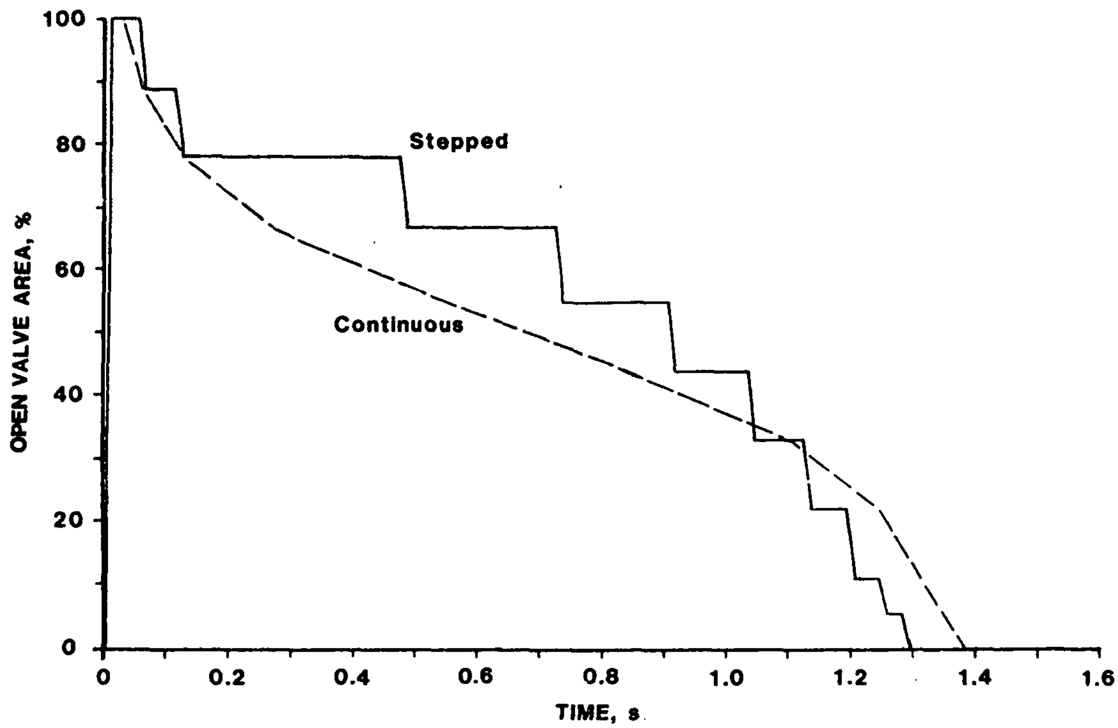

(b) Continuous and Stepped Valve Opening and Closing Functions.

Figure 13. Simulated 241 kPa & 600 kT Blast Wave

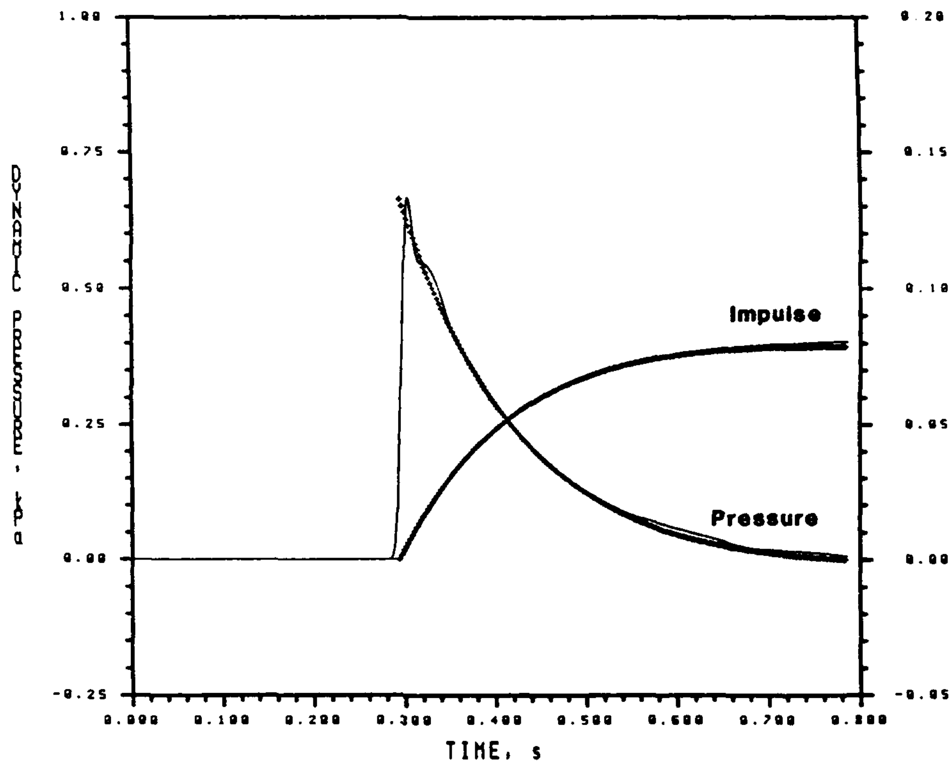

(a) Computed vs Ideal Dynamic Pressure and Impulse Histories

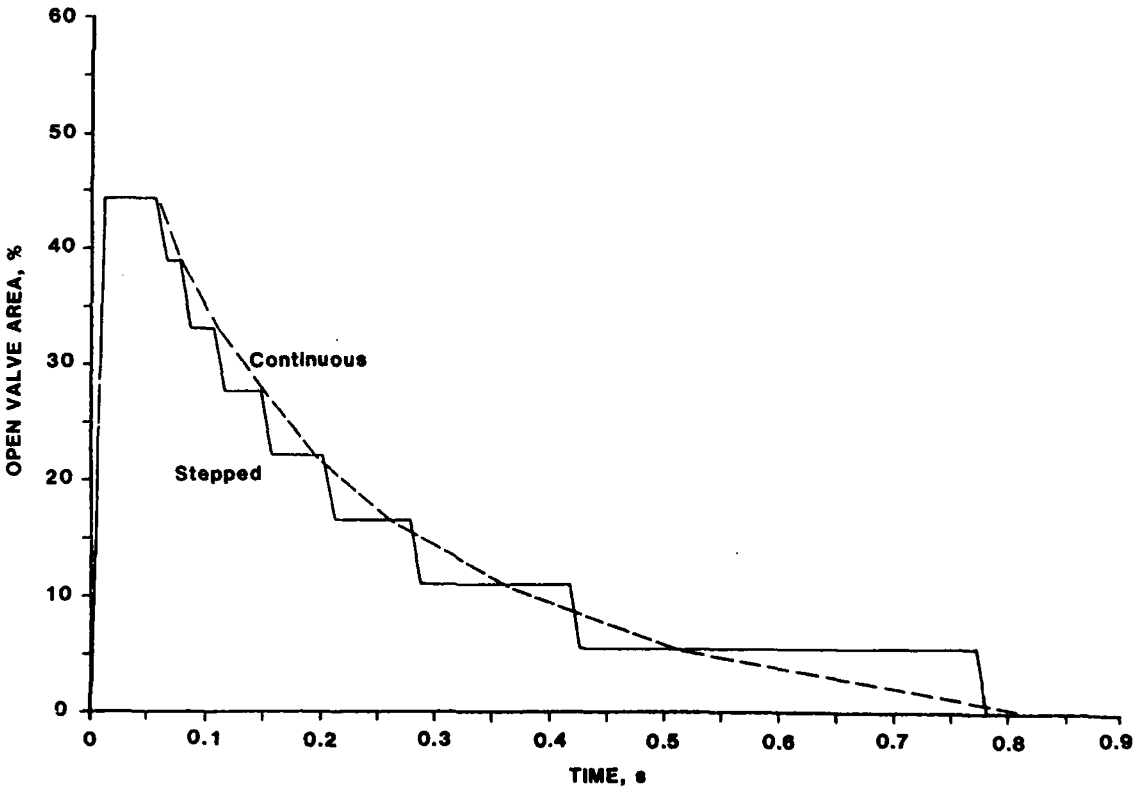

(b) Continuous and Stepped Valve Opening and Closing Functions.

Figure 14. Simulated 13.8 kPa & 1 kT Blast Wave

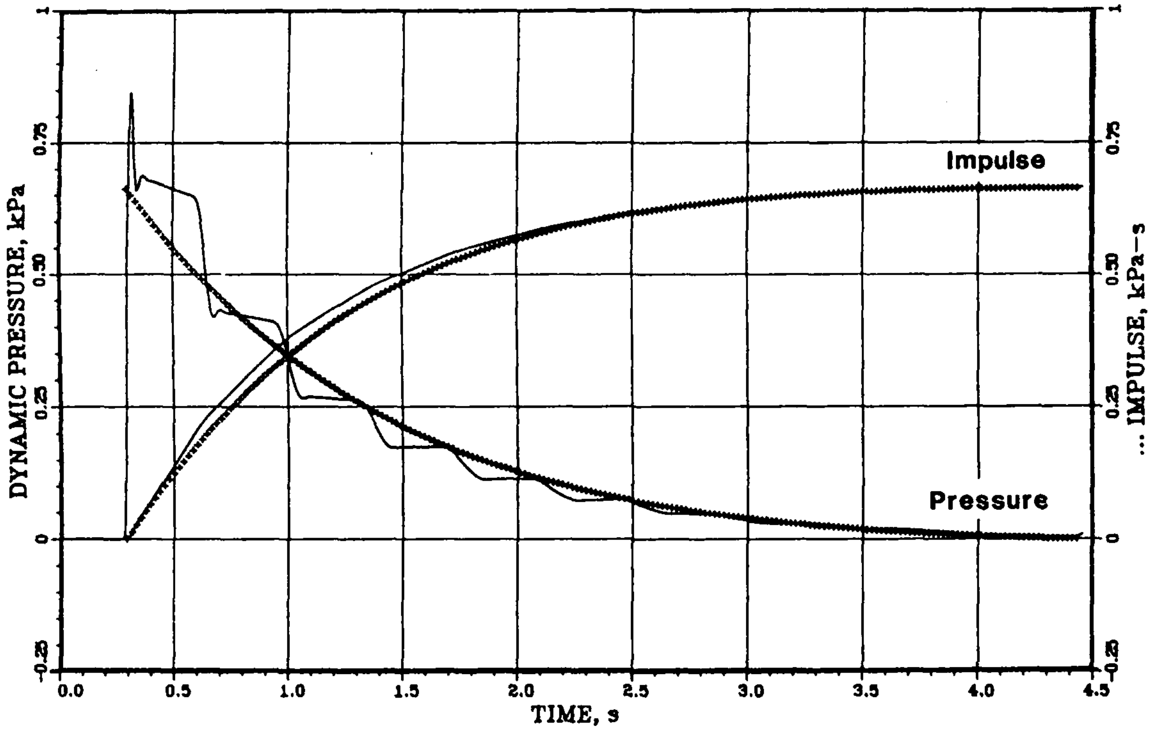

(a) Computed vs Ideal Dynamic Pressure and Impulse Histories

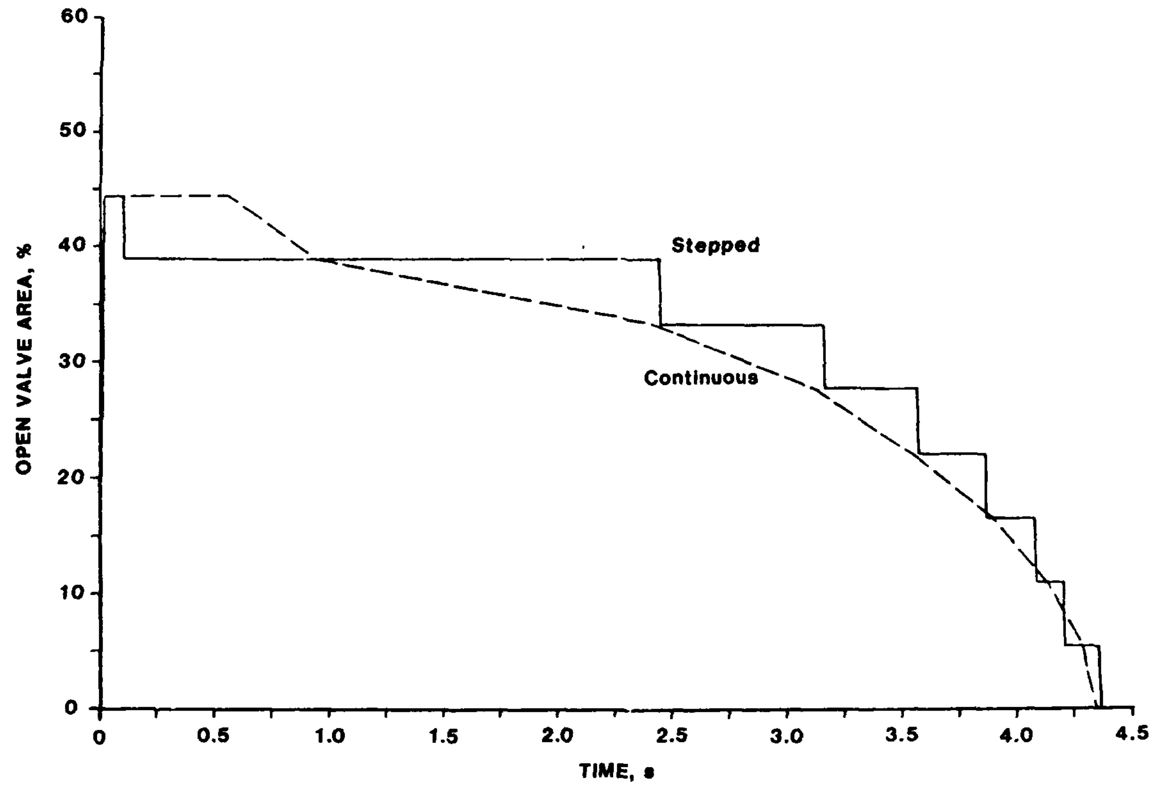

(b) Continuous and Stepped Valve Opening and Closing Functions.

Figure 15. Simulated 13.8 kPa & 600 kT Blast Wave

for the closing function between the fully open and the fully closed position of the driver throat valve, corresponding to nine valve pairs and one centrally located valve, and eight steps in the 13.8 kPa (2 psi) case where the eight open valve elements are closed individually.

Independently, and before the vendor had presented his design proposal, the previously specified continuous valve-closing functions were recomputed for an eighteen-valve assembly, and the four blast waves delimiting the operating envelope were redefined using the same procedure as described earlier. (The 19-th valve was added by the vendor to compensate for flow losses in the valves.) The resultant stepped valve-closing functions are included in Figures 12 through 15 and tabulated in Appendix B, also. Some differences particularly in the length of the delay times are apparent and were tolerated because the resultant dynamic-pressure impulse was within the stipulated tolerance range of 3% of the free-field value. The longer delay times of the continuous valve closing functions in the high-shock pressure case (241 kPa) are preferable, however, to assure that the first rarefaction wave does not catch up with the front of the blast wave before it reaches the test station.

5. CONCLUSIONS

Our computational studies with the BRL-Q1D code indicate that the advanced concepts for the drivers of the proposed full-scale LB/TS facility are feasible. The studies also show that driver heating is a necessity to realistically simulate blast waves at shock overpressures above 100 kPa. Appropriate heating of the driver gas eliminates the density discontinuity at the contact surface between the driver gas and the ambient air in the expansion tunnel. The maximum driver pressure is reduced by 40% leading to a considerable reduction of the driver wall thickness and cost savings in material. Small-scale experiments with a 1:48 scale pebble-bed heater have been completed, supporting the computational results.

Our studies further indicate that computer-controlled throat valves will have to be used if the LB/TS is to simulate the entire operational envelope. With diaphragms, the capabilities of the proposed LB/TS are significantly reduced. The upper pressure, low yield corner of the operational envelope cannot be simulated and only a limited number of discrete weapon yields can be simulated with the available driver-tube sections of finite length and number.

A conceptual design study for a 1:2 scale fast-acting throat valve consisting of nineteen digital valve elements corroborates the computational valve studies. A small-scale throat-valve model is being developed for experiments. The 1:2 scale throat valve will be used in a 1:6-scale prototype LB/TS test bed together with a pebble-bed heater and an active RWE for developmental testing. This LB/TS test bed is in the fabrication stage and, once built, will be used for proving the advanced concepts proposed for the full-scale U.S. LB/TS.

REFERENCES

[1] Gratias, S. and Monzac, J. B. G., "The Large-Scale Nuclear-Blast Simulator of the Gramat Research Center:
(1) Concept, Research, Performance;
(2) Description and Operational Utilization."
Proceedings of the Seventh International Symposium on Military Applications of Blast Simulation, Medicine Hat, Alberta, Canada, 13-17 July 1981.

[2] Mark, A., Opalka, K. O., Kitchens, C. W., Coulter, G. A., Bulmash G. and Kingery, C. N., "Simulation of Nuclear Blasts with Large-Scale Shock Tubes," Proceedings of the Eighth International Symposium on Military Applications of Blast Simulation, Spiez, Switzerland, 20-24 June 1983.

[3] Opalka, K. O., "Large Blast-Wave Simulators (LBS) With Cold-Gas Drivers: Computational Design Studies", BRL-TR-2786, US Army Ballistic Research Laboratory, Aberdeen Proving Ground, Maryland, March 1987.

[4] Ethridge, N. H., Lottero, R. E., Wortman, J. D., Bertrand, B. P., "Computational and Experimental Studies of Blockage Effects in a Blast Simulator", ARBRL-TR-02564, US Army Armament Research and Development Center, Ballistic Research Laboratory, Aberdeen Proving Ground, Maryland, June 1984

[5] Opalka, K. O. and Mark, A., "The BRL-Q1D Code: A Tool for the Numerical Simulation of Flows in Shock Tubes with Variable Cross-Sectional Areas," BRL-TR-2763, US Army Ballistic Research Laboratory, Aberdeen Proving Ground, Maryland, October 1986.

[6] Hisley, D. M., Gion, E. J. and Bertrand, B. P., "Performance and Predictions for a Large Blast Simulator Model," BRL-TR-2647, U. S. Army Ballistic Research Laboratory, Aberdeen Proving Ground, Maryland, April 1985

[7] Kingery, C. N. and Coulter, G. A., "Rarefaction Wave Eliminator Concepts for a Large Blast/Thermal Simulator", BRL-TR-2634, U. S. Army Ballistic Research Laboratory, Aberdeen Proving Ground, Maryland, February 1985

[8] Coulter, G. A., "Blast Parametric Study Using a 1:57 Scale Single Driver Model of a Large Blast Simulator", BRL-MR-3597, U. S. Army Ballistic Research Laboratory, Aberdeen Proving Ground, Maryland, June 1987

[9] Baker, W. E., ed. "Explosions in Air: Engineering Design Handbook, Part One," AMC Pamphlet No. 706-181, Headquarters, U.S. Army Material Command, Alexandria, Virginia, July 1974

[10] Beam, R. M. and Warming, R. F., "An Implicit Factored Scheme for the Compressible Navier-Stokes Equations," AIAA Journal, Vol. 16, No. 4, April 1978, pp. 393-402.

[11] Beam, R. M., and Warming, R. F., "An Implicit Factored Scheme for the Compressible Navier-Stokes Equations II: The Numerical ODE Connection," Paper No. 79-1446, AIAA 4th Computational Fluid Dynamics Conference, Williamsburgh, Virginia, 23-24 July 1979

[12] Pearson, R. J., Opalka, K. O. and Hisley D. M., "Design Studies of Drivers for the US Large Blast/Thermal Simulator," Proceedings of the Ninth International Symposium on Military Applications of Blast Simulation, Atomic Weapons Research Establishment Foulness, Southend-on-Sea, Essex, England SS3 9XE, September 1985

[13] Hisley, D. M., "Computational Studies of Wave Shaping in a Blast Simulator by Perforated Plates in the Driver," BRL-TR-2791, U.S. Army Ballistic Research Laboratory, Aberdeen Proving Ground, Maryland, March 1987

[14] Hisley, D. M., "A Computational Blast Valve Study," BRL-TR-2642, U.S. Army Ballistic Research Laboratory, Aberdeen Proving Ground, Maryland, February 1985

[15] Sverdrup Technology, Inc., "Feasibility Study of a Fast Acting Valve for the LB/TS," DNA-TR-84-394, Defense Nuclear Agency, Washington, DC, November 1984

[16] H. W. Liepmann and A. Roshko, "Elements of Gas Dynamics," pgs. 79-81, John Wiley & Sons, Inc., New York, New York, 1963

[17] The IMSL Library, Library Reference Manual, Volume 2, International Mathematical & Statistical Libraries, Inc. 7500 Bellaire Boulevard, Houston, Texas, USA, Edition 8, June 1980

[18] Pearson, R. J., "Large Blast/Thermal Simulation," SAE Technical Paper #871746, Society of Automotive Engineers, 400 Commonwealth Drive, Warrendale, Pennsylvania, October 1987

[19] Barry, R. A. and Lassahn G. D., "Valve Opening-Time Requirements for LB/TS", EG&G Idaho, Inc. (INEL), Contractor Report BRL-CR-602, U.S. Army LABCOM Ballistic Research Laboratory, Aberdeen Proving Ground, Maryland , November 1988

[20] Reed, T. R., "Conceptual Valve Design for the Driver Tube of the Large Blast/Thermal Simulator," Contractor Report BRL-CR-610, U.S. Army LABCOM Ballistic Research Laboratory, Aberdeen Proving Ground, Maryland , May 1989

ACKNOWLEDGEMENT

The Author wishes to acknowledge the contribution of Mr. Stephen B. Schramel who converted the plotting routines for the BRL-Q1D code from DISSPLA to PVI software in a short time and then efficiently completed the valve closing computations.

APPENDIX A

LB/TS DRIVER INITIAL CONDITIONS FOR HEATED GAS

INITIAL DRIVER CONDITIONS FOR THE ADVANCED-CONCEPT LB/TS DESIGN

p_{so} *kPa*	p_{so} *psi*	P_{21}	P_{41}	T_{41}
1.0	0.145	1.010	1.312	1.001
2.0	0.290	1.020	1.670	1.004
3.0	0.435	1.030	2.041	1.007
4.0	0.580	1.039	2.423	1.010
5.0	0.725	1.049	2.817	1.013
6.0	0.870	1.059	3.222	1.016
7.0	1.015	1.069	3.638	1.019
8.0	1.160	1.079	4.064	1.022
9.0	1.305	1.089	4.500	1.025
10.0	1.450	1.099	4.946	1.028
11.0	1.595	1.109	5.401	1.031
12.0	1.740	1.118	5.866	1.035
13.0	1.885	1.128	6.339	1.038
14.0	2.031	1.138	6.821	1.041
15.0	2.176	1.148	7.311	1.044
16.0	2.321	1.158	7.808	1.047
17.0	2.466	1.168	8.313	1.050
18.0	2.611	1.178	8.826	1.053
19.0	2.756	1.188	9.345	1.057
20.0	2.901	1.197	9.870	1.060
21.0	3.046	1.207	10.40	1.063
22.0	3.191	1.217	10.94	1.066
23.0	3.336	1.227	11.48	1.070
24.0	3.481	1.237	12.03	1.073
25.0	3.626	1.247	12.58	1.076
26.0	3.771	1.257	13.14	1.079
27.0	3.916	1.266	13.70	1.083
28.0	4.061	1.276	14.26	1.086
29.0	4.206	1.286	14.83	1.089
30.0	4.351	1.296	15.40	1.093
31.0	4.496	1.306	15.98	1.096
32.0	4.641	1.316	16.55	1.100
33.0	4.786	1.326	17.13	1.103
34.0	4.931	1.336	17.71	1.107
35.0	5.076	1.345	18.29	1.110

NOMENCLATURE:

p_{so} - shock overpressure

P_{21} - shock pressure ratio

P_{41} - diaphragm pressure ratio

T_{41} - diaphragm temperature ratio

INITIAL DRIVER CONDITIONS
FOR THE ADVANCED-CONCEPT LB/TS DESIGN

p_{so} *kPa*	p_{so} *psi*	P_{21}	P_{41}	T_{41}
36.0	5.221	1.355	18.88	1.114
37.0	5.366	1.365	19.46	1.117
38.0	5.511	1.375	20.04	1.121
39.0	5.656	1.385	20.63	1.124
40.0	5.802	1.395	21.21	1.128
41.0	5.947	1.405	21.79	1.131
42.0	6.092	1.415	22.38	1.135
43.0	6.237	1.424	22.96	1.139
44.0	6.382	1.434	23.54	1.142
45.0	6.527	1.444	24.11	1.146
46.0	6.672	1.454	24.69	1.150
47.0	6.817	1.464	25.26	1.154
48.0	6.962	1.474	25.83	1.158
49.0	7.107	1.484	26.40	1.161
50.0	7.252	1.493	26.96	1.165
51.0	7.397	1.503	27.52	1.169
52.0	7.542	1.513	28.08	1.173
53.0	7.687	1.523	28.64	1.177
54.0	7.832	1.533	29.19	1.181
55.0	7.977	1.543	29.74	1.185
56.0	8.122	1.553	30.29	1.189
57.0	8.267	1.563	30.84	1.193
58.0	8.412	1.572	31.38	1.197
59.0	8.557	1.582	31.92	1.201
60.0	8.702	1.592	32.46	1.206
61.0	8.847	1.602	33.00	1.210
62.0	8.992	1.612	33.53	1.214
63.0	9.137	1.622	34.06	1.218
64.0	9.282	1.632	34.59	1.223
65.0	9.427	1.642	35.12	1.227
66.0	9.572	1.651	35.64	1.231
67.0	9.718	1.661	36.17	1.236
68.0	9.863	1.671	36.69	1.240
69.0	10.01	1.681	37.20	1.245
70.0	10.15	1.691	37.72	1.249

NOMENCLATURE:

p_{so} - shock overpressure
P_{21} - shock pressure ratio
P_{41} - diaphragm pressure ratio
T_{41} - diaphragm temperature ratio

INITIAL DRIVER CONDITIONS
FOR THE ADVANCED-CONCEPT LB/TS DESIGN

p_{so}		P_{21}	P_{41}	T_{41}
kPa	*psi*			
70.5	10.23	1.696	37.98	1.252
71.0	10.30	1.701	38.24	1.254
71.5	10.37	1.706	38.49	1.256
72.0	10.44	1.711	38.75	1.258
72.5	10.52	1.716	39.00	1.261
73.0	10.59	1.720	39.26	1.263
73.5	10.66	1.725	39.51	1.265
74.0	10.73	1.730	39.76	1.268
74.5	10.81	1.735	40.02	1.270
75.0	10.88	1.740	40.27	1.272
75.5	10.95	1.745	40.52	1.275
76.0	11.02	1.750	40.77	1.277
76.5	11.10	1.755	41.02	1.279
77.0	11.17	1.760	41.27	1.282
77.5	11.24	1.765	41.52	1.284
78.0	11.31	1.770	41.77	1.286
78.5	11.39	1.775	42.02	1.289
79.0	11.46	1.780	42.27	1.291
79.5	11.53	1.785	42.52	1.293
80.0	11.60	1.790	42.77	1.296
80.5	11.68	1.794	43.01	1.298
81.0	11.75	1.799	43.26	1.301
81.5	11.82	1.804	43.51	1.303
82.0	11.89	1.809	43.75	1.305
82.5	11.97	1.814	44.00	1.308
83.0	12.04	1.819	44.24	1.310
83.5	12.11	1.824	44.49	1.313
84.0	12.18	1.829	44.73	1.315
84.5	12.26	1.834	45.97	1.318
85.0	12.33	1.839	45.22	1.320
85.5	12.40	1.844	45.46	1.323
86.0	12.47	1.849	45.70	1.325
86.5	12.55	1.854	45.94	1.327
87.0	12.62	1.859	46.19	1.330
87.5	12.69	1.864	46.43	1.332

NOMENCLATURE:
p_{so} - shock overpressure
P_{21} - shock pressure ratio
P_{41} - diaphragm pressure ratio
T_{41} - diaphragm temperature ratio

INITIAL DRIVER CONDITIONS
FOR THE ADVANCED-CONCEPT LB/TS DESIGN

p_{so} *kPa*	p_{so} *psi*	P_{21}	P_{41}	T_{41}
88.0	12.76	1.868	46.67	1.335
88.5	12.84	1.873	46.91	1.337
89.0	12.91	1.878	47.15	1.340
89.5	12.98	1.883	47.39	1.342
90.0	13.05	1.888	47.63	1.345
90.5	13.13	1.893	47.87	1.347
91.0	13.20	1.898	48.10	1.350
91.5	13.27	1.903	48.34	1.352
92.0	13.34	1.908	48.58	1.355
92.5	13.42	1.913	48.82	1.358
93.0	13.49	1.918	49.05	1.360
93.5	13.56	1.923	49.29	1.363
94.0	13.63	1.928	49.52	1.365
94.5	13.71	1.933	49.76	1.368
95.0	13.78	1.938	50.00	1.370
95.5	13.85	1.943	50.23	1.373
96.0	13.92	1.947	50.47	1.375
96.5	14.00	1.952	50.70	1.378
97.0	14.07	1.957	50.93	1.381
97.5	14.14	1.962	51.17	1.383
98.0	14.21	1.967	51.40	1.386
98.5	14.29	1.972	51.63	1.388
99.0	14.36	1.977	51.86	1.391
99.5	14.43	1.982	52.10	1.394
100.0	14.50	1.987	52.33	1.396
100.5	14.58	1.992	52.56	1.399
101.0	14.65	1.997	52.79	1.401
101.5	14.72	2.002	53.02	1.404
102.0	14.79	2.007	53.25	1.407
102.5	14.87	2.012	53.48	1.409
103.0	14.94	2.017	53.71	1.412
103.5	15.01	2.021	53.94	1.415
104.0	15.08	2.026	54.17	1.417
104.5	15.16	2.031	54.40	1.420
105.0	15.23	2.036	54.63	1.423

NOMENCLATURE:

p_{so} - shock overpressure

P_{21} - shock pressure ratio

P_{41} - diaphragm pressure ratio

T_{41} - diaphragm temperature ratio

INITIAL DRIVER CONDITIONS
FOR THE ADVANCED-CONCEPT LB/TS DESIGN

p_{so} *kPa*	p_{so} *psi*	P_{21}	P_{41}	T_{41}
105.5	15.30	2.041	54.86	1.425
106.0	15.37	2.046	55.09	1.428
106.5	15.45	2.051	55.31	1.431
107.0	15.52	2.056	55.54	1.433
107.5	15.59	2.061	55.77	1.436
108.0	15.66	2.066	56.00	1.439
108.5	15.74	2.071	56.22	1.441
109.0	15.81	2.076	56.45	1.444
109.5	15.88	2.081	56.67	1.447
110.0	15.95	2.086	56.90	1.449
110.5	16.03	2.091	57.13	1.452
111.0	16.10	2.095	57.35	1.455
111.5	16.17	2.100	57.58	1.458
112.0	16.24	2.105	57.80	1.460
112.5	16.32	2.110	58.03	1.463
113.0	16.39	2.115	58.25	1.466
113.5	16.46	2.120	58.48	1.468
114.0	16.53	2.125	58.70	1.471
114.5	16.61	2.130	58.92	1.474
115.0	16.68	2.135	59.15	1.477
115.5	16.75	2.140	59.37	1.479
116.0	16.82	2.145	59.59	1.482
116.5	16.90	2.150	59.82	1.485
117.0	16.97	2.155	60.04	1.488
117.5	17.04	2.160	60.26	1.490
118.0	17.11	2.165	60.48	1.493
118.5	17.19	2.170	60.71	1.496
119.0	17.26	2.174	60.93	1.499
119.5	17.33	2.179	61.15	1.501
120.0	17.40	2.184	61.37	1.504
120.5	17.48	2.189	61.59	1.507
121.0	17.55	2.194	61.81	1.510
121.5	17.62	2.199	62.03	1.513
122.0	17.69	2.204	62.25	1.515
122.5	17.77	2.209	62.47	1.518

NOMENCLATURE:

p_{so} - shock overpressure

P_{21} - shock pressure ratio

P_{41} - diaphragm pressure ratio

T_{41} - diaphragm temperature ratio

INITIAL DRIVER CONDITIONS

FOR THE ADVANCED-CONCEPT LB/TS DESIGN

p_{so} *kPa*	p_{so} *psi*	P_{21}	P_{41}	T_{41}
123.0	17.84	2.214	62.70	1.521
123.5	17.91	2.219	62.92	1.524
124.0	17.98	2.224	63.14	1.526
124.5	18.06	2.229	63.36	1.529
125.0	18.13	2.234	63.57	1.531
125.5	18.20	2.239	63.79	1.535
126.0	18.27	2.244	64.01	1.538
126.5	18.35	2.248	64.23	1.541
127.0	18.42	2.253	64.45	1.543
127.5	18.49	2.258	64.67	1.546
128.0	18.56	2.263	64.89	1.549
128.5	18.64	2.268	65.11	1.552
129.0	18.71	2.273	65.33	1.555
129.5	18.78	2.278	65.55	1.557
130.0	18.85	2.283	65.76	1.560
130.5	18.93	2.288	65.98	1.563
131.0	19.00	2.293	66.20	1.566
131.5	19.07	2.298	66.42	1.569
132.0	19.14	2.303	66.64	1.572
132.5	19.22	2.308	66.85	1.574
133.0	19.29	2.313	67.07	1.577
133.5	19.36	2.318	67.29	1.580
134.0	19.44	2.322	67.51	1.583
134.5	19.51	2.327	67.72	1.586
135.0	19.58	2.332	67.94	1.589
135.5	19.65	2.337	68.16	1.592
136.0	19.73	2.342	68.38	1.594
136.5	19.80	2.347	68.59	1.597
137.0	19.87	2.352	68.81	1.600
137.5	19.94	2.357	69.03	1.603
138.0	20.02	2.362	69.24	1.606
138.5	20.09	2.367	69.46	1.609
139.0	20.16	2.372	69.68	1.612
139.5	20.23	2.377	69.89	1.614
140.0	20.30	2.382	70.11	1.617

NOMENCLATURE:

p_{so} - shock overpressure

P_{21} - shock pressure ratio

P_{41} - diaphragm pressure ratio

T_{41} - diaphragm temperature ratio

INITIAL DRIVER CONDITIONS
FOR THE ADVANCED-CONCEPT LB/TS DESIGN

p_{so} *kPa*	p_{so} *psi*	P_{21}	P_{41}	T_{41}
140.5	20.38	2.387	70.33	1.620
141.0	20.45	2.392	70.54	1.623
141.5	20.52	2.396	70.76	1.626
142.0	20.60	2.401	70.98	1.629
142.5	20.67	2.406	71.19	1.632
143.0	20.74	2.411	71.41	1.634
143.5	20.81	2.416	71.63	1.637
144.0	20.89	2.421	71.84	1.640
144.5	20.96	2.426	72.06	1.643
145.0	21.03	2.431	72.28	1.646
145.5	21.10	2.436	72.49	1.649
146.0	21.18	2.441	72.71	1.652
146.5	21.25	2.446	72.92	1.655
147.0	21.32	2.451	73.14	1.658
147.5	21.39	2.456	73.36	1.660
148.0	21.47	2.461	73.57	1.663
148.5	21.54	2.466	73.79	1.666
149.0	21.61	2.471	74.01	1.669
149.5	21.68	2.475	74.22	1.672
150.0	21.76	2.480	74.44	1.675
150.5	21.83	2.485	74.65	1.678
151.0	21.90	2.490	74.87	1.681
151.5	21.97	2.495	75.09	1.684
152.0	22.05	2.500	75.30	1.686
152.5	22.12	2.505	75.52	1.689
153.0	22.19	2.510	75.74	1.692
153.5	22.26	2.515	75.95	1.695
154.0	22.34	2.520	76.17	1.698
154.5	22.41	2.525	76.39	1.701
155.0	22.48	2.530	76.60	1.704
155.5	22.55	2.535	76.82	1.707
156.0	22.63	2.540	77.04	1.710
156.5	22.70	2.545	77.25	1.712
157.0	22.77	2.549	77.47	1.715
157.5	22.84	2.554	77.69	1.718

NOMENCLATURE:

p_{so} - shock overpressure

P_{21} - shock pressure ratio

P_{41} - diaphragm pressure ratio

T_{41} - diaphragm temperature ratio

INITIAL DRIVER CONDITIONS
FOR THE ADVANCED-CONCEPT LB/TS DESIGN

p_{so} *kPa*	p_{so} *psi*	P_{21}	P_{41}	T_{41}
158.0	22.92	2.559	77.90	1.721
158.5	22.99	2.564	78.12	1.724
159.0	23.06	2.569	78.34	1.727
159.5	23.13	2.574	78.56	1.730
160.0	23.21	2.579	78.77	1.733
160.5	23.28	2.584	78.99	1.736
161.0	23.35	2.589	79.21	1.739
161.5	23.42	2.594	79.43	1.741
162.0	23.50	2.599	79.64	1.744
162.5	23.57	2.604	79.86	1.747
163.0	23.64	2.609	80.08	1.750
163.5	23.71	2.614	80.30	1.753
164.0	23.79	2.619	80.51	1.756
164.5	23.86	2.623	80.73	1.759
165.0	23.93	2.628	80.95	1.762
165.5	24.00	2.633	81.17	1.765
166.0	24.08	2.638	81.39	1.767
166.5	24.15	2.643	81.61	1.770
167.0	24.22	2.648	81.83	1.773
167.5	24.29	2.653	82.05	1.776
168.0	24.37	2.658	82.26	1.779
168.5	24.44	2.663	82.48	1.782
169.0	24.51	2.668	82.70	1.785
169.5	24.58	2.673	82.92	1.788
170.0	24.66	2.678	83.14	1.791
170.5	24.73	2.683	83.36	1.793
171.0	24.80	2.688	83.58	1.796
171.5	24.87	2.693	83.80	1.799
172.0	24.95	2.698	84.02	1.802
172.5	25.02	2.703	84.24	1.805
173.0	25.09	2.707	84.46	1.808
173.5	25.16	2.712	84.69	1.811
174.0	25.24	2.717	84.91	1.814
174.5	25.31	2.722	85.13	1.817
175.0	25.38	2.727	85.35	1.819

NOMENCLATURE:
p_{so} - shock overpressure
P_{21} - shock pressure ratio
P_{41} - diaphragm pressure ratio
T_{41} - diaphragm temperature ratio

INITIAL DRIVER CONDITIONS
FOR THE ADVANCED-CONCEPT LB/TS DESIGN

p_{so} *kPa*	p_{so} *psi*	P_{21}	P_{41}	T_{41}
175.5	25.45	2.732	85.57	1.822
176.0	25.53	2.737	85.79	1.825
176.5	25.60	2.742	86.02	1.828
177.0	25.67	2.747	86.24	1.831
177.5	25.74	2.752	86.46	1.834
178.0	25.82	2.757	86.68	1.837
178.5	25.89	2.762	86.91	1.840
179.0	25.96	2.767	87.13	1.842
179.5	26.03	2.772	87.35	1.845
180.0	26.11	2.776	87.58	1.848
180.5	26.18	2.781	87.80	1.851
181.0	26.25	2.786	88.02	1.854
181.5	26.32	2.791	88.25	1.857
182.0	26.40	2.796	88.47	1.860
182.5	26.47	2.801	88.70	1.862
183.0	26.54	2.806	88.92	1.865
183.5	26.61	2.811	89.15	1.868
184.0	26.69	2.816	89.37	1.871
184.5	26.76	2.821	89.60	1.874
185.0	26.83	2.826	89.82	1.877
185.5	26.90	2.831	90.05	1.879
186.0	26.98	2.836	90.28	1.882
186.5	27.05	2.841	90.50	1.885
187.0	27.12	2.846	90.73	1.888
187.5	27.19	2.850	90.96	1.891
188.0	27.27	2.855	91.19	1.894
188.5	27.34	2.860	91.41	1.896
189.0	27.41	2.865	91.64	1.899
189.5	27.48	2.870	91.87	1.902
190.0	27.56	2.875	92.10	1.905
190.5	27.63	2.880	92.33	1.908
191.0	27.70	2.885	92.56	1.911
191.5	27.77	2.890	92.79	1.913
192.0	27.85	2.895	93.02	1.916
192.5	27.92	2.900	93.25	1.919

NOMENCLATURE:
p_{so} - shock overpressure
P_{21} - shock pressure ratio
P_{41} - diaphragm pressure ratio
T_{41} - diaphragm temperature ratio

INITIAL DRIVER CONDITIONS
FOR THE ADVANCED-CONCEPT LB/TS DESIGN

p_{so} *kPa*	p_{so} *psi*	P_{21}	P_{41}	T_{41}
193.0	27.99	2.905	93.48	1.922
193.5	28.06	2.910	93.71	1.925
194.0	28.14	2.915	93.94	1.927
194.5	28.21	2.920	94.17	1.930
195.0	28.28	2.925	94.40	1.933
195.5	28.35	2.929	94.64	1.936
196.0	28.43	2.934	94.87	1.939
196.5	28.50	2.939	95.10	1.941
197.0	28.57	2.944	95.33	1.944
197.5	28.64	2.949	95.57	1.947
198.0	28.72	2.954	95.80	1.950
198.5	28.79	2.959	96.04	1.952
199.0	28.86	2.964	96.27	1.955
199.5	28.94	2.969	96.51	1.958
200.0	29.01	2.974	96.74	1.961
200.5	29.08	2.979	96.98	1.963
201.0	29.15	2.984	97.21	1.966
201.5	29.23	2.989	97.45	1.969
202.0	29.30	2.994	97.69	1.972
202.5	29.37	2.999	97.92	1.974
203.0	29.44	3.003	98.16	1.977
203.5	29.52	3.008	98.40	1.980
204.0	29.59	3.013	98.64	1.983
204.5	29.66	3.018	98.88	1.985
205.0	29.73	3.023	99.11	1.988
205.5	29.81	3.028	99.35	1.991
206.0	29.88	3.033	99.59	1.994
206.5	29.95	3.038	99.83	1.996
207.0	30.02	3.043	100.08	1.999
207.5	30.10	3.048	100.32	2.002
208.0	30.17	3.053	100.56	2.004
208.5	30.24	3.058	100.80	2.007
209.0	30.31	3.063	101.04	2.010
209.5	30.39	3.068	101.29	2.012
210.0	30.46	3.073	101.53	2.015

NOMENCLATURE:
p_{so} - shock overpressure
P_{21} - shock pressure ratio
P_{41} - diaphragm pressure ratio
T_{41} - diaphragm temperature ratio

INITIAL DRIVER CONDITIONS
FOR THE ADVANCED-CONCEPT LB/TS DESIGN

p_{so} *kPa*	p_{so} *psi*	P_{21}	P_{41}	T_{41}
210.5	30.53	3.077	101.77	2.018
211.0	30.60	3.082	102.02	2.021
211.5	30.68	3.087	102.26	2.023
212.0	30.75	3.092	102.51	2.026
212.5	30.82	3.097	102.75	2.029
213.0	30.89	3.102	103.00	2.031
213.5	30.97	3.107	103.24	2.034
214.0	31.04	3.112	103.49	2.036
214.5	31.11	3.117	103.74	2.039
215.0	31.18	3.122	103.99	2.042
215.5	31.25	3.127	104.23	2.044
216.0	31.33	3.132	104.48	2.047
216.5	31.40	3.137	104.73	2.050
217.0	31.47	3.142	104.98	2.052
217.5	31.54	3.147	105.23	2.055
218.0	31.62	3.151	105.48	2.058
218.5	31.69	3.156	105.73	2.060
219.0	31.76	3.161	105.98	2.063
219.5	31.84	3.166	106.24	2.065
220.0	31.91	3.171	106.49	2.068
220.5	31.98	3.176	106.74	2.071
221.0	32.05	3.181	107.00	2.073
221.5	32.13	3.186	107.25	2.076
222.0	32.20	3.191	107.50	2.078
222.5	32.27	3.196	107.76	2.081
223.0	32.34	3.201	108.02	2.083
223.5	32.42	3.206	108.27	2.086
224.0	32.49	3.211	108.53	2.089
224.5	32.56	3.216	108.79	2.091
225.0	32.63	3.221	109.04	2.094
225.5	32.71	3.226	109.30	2.096
226.0	32.78	3.230	109.56	2.099
226.5	32.85	3.235	109.82	2.101
227.0	32.92	3.240	110.08	2.104
227.5	33.00	3.245	110.34	2.106

NOMENCLATURE:
p_{so} - shock overpressure
P_{21} - shock pressure ratio
P_{41} - diaphragm pressure ratio
T_{41} - diaphragm temperature ratio

INITIAL DRIVER CONDITIONS
FOR THE ADVANCED-CONCEPT LB/TS DESIGN

p_{so} *kPa*	*psi*	P_{21}	P_{41}	T_{41}
228.0	33.07	3.250	110.60	2.109
228.5	33.14	3.255	110.86	2.111
229.0	33.21	3.260	111.13	2.114
229.5	33.29	3.265	111.39	2.116
230.0	33.36	3.270	111.65	2.119
230.5	33.43	3.275	111.91	2.121
231.0	33.50	3.280	112.18	2.124
231.5	33.58	3.285	112.44	2.126
232.0	33.65	3.290	112.71	2.129
232.5	33.72	3.295	112.98	2.131
233.0	33.79	3.300	113.24	2.134
233.5	33.87	3.304	113.51	2.136
234.0	33.94	3.309	113.78	2.138
234.5	34.01	3.314	114.05	2.141
235.0	34.08	3.319	114.32	2.143
235.5	34.16	3.324	114.59	2.146
236.0	34.23	3.329	114.86	2.148
236.5	34.30	3.334	115.13	2.151
237.0	34.37	3.339	115.40	2.153
237.5	34.45	3.344	115.67	2.155
238.0	34.52	3.349	115.94	2.158
238.5	34.59	3.354	116.22	2.160
239.0	34.66	3.359	116.49	2.163
239.5	34.74	3.364	116.77	2.165
240.0	34.81	3.369	117.04	2.167
240.5	34.88	3.374	117.32	2.170
241.0	34.95	3.378	117.59	2.172
241.5	35.03	3.383	117.87	2.174
242.0	35.10	3.388	118.15	2.177
242.5	35.17	3.393	118.43	2.179
243.0	35.24	3.398	118.71	2.181
243.5	35.32	3.403	118.99	2.184
244.0	35.39	3.408	119.27	2.186
244.5	35.46	3.413	119.55	2.188
245.0	35.53	3.418	119.83	2.191

NOMENCLATURE:
p_{so} - shock overpressure
P_{21} - shock pressure ratio
P_{41} - diaphragm pressure ratio
T_{41} - diaphragm temperature ratio

APPENDIX B

LB/TS DRIVER THROAT VALVE CLOSING FUNCTIONS

TABLE I. CONTINUOUS VALVE CLOSINC FUNCTION FOR A **241kPa & 1kT** BLAST WAVE		
A_V %	Δt *ms*	t *s*
0.0	0	0.0
100.0	10	0.010
100.0	40	0.050
96.00	4	0.054
67.50	4	0.058
47.40	4	0.062
24.40	6	0.068
13.30	8	0.076
7.42	10	0.086
4.24	10	0.096
1.40	20	0.116
0.50	20	0.136
0.0	20	0.156
Valve closed to end of computation.		

NOMENCLATURE:

t - time from beginning of test, in seconds

Δt - time increment, in milliseconds

A_V - total open valve area in % of throat area

TABLE II.
STEPPED VALVE CLOSING FUNCTION
FOR A **241kPa & 1kT** BLAST WAVE

A_V %	N_V	Δt *ms*	t *s*
0.0	0	0	0.0
100.0	18	10	0.010
		25	0.035
55.56	10	10	0.045
		5	0.050
33.33	6	10	0.060
		5	0.065
16.67	3	10	0.075
		5	0.080
5.556	1	10	0.090
		55	0.145
0.0	0	10	0.155
All valves closed to end of computation.			

NOMENCLATURE:
t - time from beginning of test, in seconds
Δt - time increment, in milliseconds
N_V - number of open valves
A_V - total open valve area in % of throat area

TABLE III.
CONTINUOUS VALVE CLOSING FUNCTION
FOR A **241kPa & 600kT** BLAST WAVE

A_V %	Δt *ms*	t *s*
0.0	0	0.0
100.0	10	0.010
100.0	15	0.025
88.89	45	0.060
77.78	65	0.125
66.67	145	0.270
55.56	260	0.530
44.44	310	0.840
33.33	260	1.100
22.22	145	1.245
11.11	65	1.310
5.56	45	1.355
0.0	25	1.380
Valve closed to end of computation.		

NOMENCLATURE:
t - **time from beginning of test, in seconds**
Δt - **time increment, in milliseconds**
A_V - **total open valve area in % of throat area**

TABLE IV.
STEPPED VALVE CLOSING FUNCTION
FOR A **241kPa & 600kT** BLAST WAVE

A_V %	N_V	Δt *ms*	t *s*
0.0	0	0	0.0
100.0	18	10	0.010
		45	0.055
88.89	16	10	0.065
		50	0.115
77.78	14	10	0.125
		350	0.475
66.67	12	10	0.485
		240	0.725
55.56	10	10	0.735
		170	0.905
44.44	8	10	0.915
		120	1.035
33.33	6	10	1.045
		80	1.125
22.22	4	10	1.135
		60	1.195
11.11	2	10	1.205
		40	1.245
5.56	1	10	1.255
		30	1.285
0.0	0	10	1.295

All valves closed to end of computation.

NOMENCLATURE:
t - time from beginning of test, in seconds
Δt - time increment, in milliseconds
N_V - number of open valves
A_V - total open valve area in % of throat area

TABLE V.
CONTINUOUS VALVE CLOSING FUNCTION
FOR A **13.8kPa & 1kT** BLAST WAVE

A_V %	Δt *ms*	t *s*
0.0	0	0.0
44.44	10	0.010
44.44	45	0.055
38.89	20	0.075
33.33	35	0.110
27.78	40	0.150
22.22	45	0.195
16.67	65	0.260
11.11	100	0.360
5.56	150	0.510
0.0	300	0.810

Valve closed to end of computation.

NOMENCLATURE:
t - time from beginning of test, in seconds
Δt - time increment, in milliseconds
A_V - total open valve area in % of throat area

TABLE VI.
STEPPED VALVE CLOSING FUNCTION
FOR A **13.8kPa & 1kT** BLAST WAVE

A_V %	N_V	Δt *ms*	t *s*
0.0	0	0	0.0
44.44	8	10	0.010
		45	0.055
38.89	7	10	0.065
		12	0.077
33.33	6	10	0.087
		20	0.107
27.78	5	10	0.117
		30	0.147
22.22	4	10	0.157
		45	0.202
16.67	3	10	0.212
		65	0.277
11.11	2	10	0.287
		130	0.417
5.56	1	10	0.427
		345	0.772
0.0	0	10	0.782
All valves closed to end of computation.			

NOMENCLATURE:
t - time from beginning of test, in seconds
Δt - time increment, in milliseconds
N_V - number of open valves
A_V - total open valve area in % of throat area

TABLE VII.

CONTINUOUS VALVE CLOSING FUNCTION
FOR A **13.8kPa & 600kT** BLAST WAVE

A_V %	Δt *ms*	t *s*
0.00	0	0.000
44.44	10	0.010
44.44	45	0.055
38.89	75	0.930
33.33	1460	2.390
27.78	740	3.130
22.22	450	3.580
16.67	325	3.905
11.11	225	4.130
5.56	150	4.280
0.00	90	4.370
Valve closed to end of computation.		

NOMENCLATURE:
t - time from beginning of test, in seconds
Δt - time increment, in milliseconds
A_V - total open valve area in % of throat area

TABLE VIII.
STEPPED VALVE CLOSING FUNCTION
FOR A **13.8kPa & 600kT** BLAST WAVE

A_V %	N_V	Δt *ms*	t *s*
0.0	0	0	0.000
44.44	8	10	0.010
		85	0.095
38.89	7	10	0.105
		2325	2.430
33.33	6	10	2.440
		715	3.155
27.78	5	10	3.165
		395	3.560
22.22	4	10	3.570
		295	3.865
16.67	3	10	3.875
		195	4.070
11.11	2	10	4.080
		145	4.225
5.56	1	10	4.235
		125	4.360
0.0	0	10	4.370

All valves closed to end of computation.

NOMENCLATURE:
t - time from beginning of test, in seconds
Δt - time increment, in milliseconds
N_V - number of open valves
A_V - total open valve area in % of throat area

No of Copies	Organization
(Unclass., unlimited) 12 (Unclass., limited) 2 (Classified) 2	Administrator Defense Technical Info Center ATTN: DTIC-DDA Cameron Station Alexandria, VA 22304-6145
1	HQDA (SARD-TR) WASH, DC 20310-0001
1	Commander US Army Materiel Command ATTN: AMCDRA-ST 5001 Eisenhower Avenue Alexandria, VA 22333-0001
1	Commander US Army Laboratory Command ATTN: AMSLC-DL Adelphi, MD 20783-1145
2	Commander Armament RD&E Center US Army AMCCOM ATTN: SMCAR-MSI Picatinny Arsenal, NJ 07806-5000
2	Commander Armament RD&E Center US Army AMCCOM ATTN: SMCAR-TDC Picatinny Arsenal, NJ 07806-5000
1	Director Benet Weapons Laboratory Armament RD&E Center US Army AMCCOM ATTN: SMCAR-LCB-TL Watervliet, NY 12189-4050
1	Commander US Army Armament, Munitions and Chemical Command ATTN: SMCAR-ESP-L Rock Island, IL 61299-5000
1	Commander US Army Aviation Systems Command ATTN: AMSAV-DACL 4300 Goodfellow Blvd. St. Louis, MO 63120-1798
1	Director US Army Aviation Research and Technology Activity Ames Research Center Moffett Field, CA 94035-1099

No of Copies	Organization
1	Commander US Army Missile Command ATTN: AMSMI-RD-CS-R (DOC) Redstone Arsenal, AL 35898-5010
1	Commander US Army Tank Automotive Command ATTN: AMSTA-TSL (Technical Library) Warren, MI 48397-5000
1	Director US Army TRADOC Analysis Command ATTN: ATAA-SL White Sands Missile Range, NM 88002-5502
(Class. only) 1	Commandant US Army Infantry School ATTN: ATSH-CD (Security Mgr.) Fort Benning, GA 31905-5660
(Unclass. only) 1	Commandant US Army Infantry School ATTN: ATSH-CD-CSO-OR Fort Benning, GA 31905-5660
1	The Rand Corporation P.O. Box 2138 Santa Monica, CA 90401-2138
(Class. only) 1	Air Force Armament Laboratory ATTN: AFATL/DLODL Eglin AFB, FL 32542-5000
	Aberdeen Proving Ground Dir, USAMSAA ATTN: AMXSY-D AMXSY-MP, H. Cohen Cdr, USATECOM ATTN: AMSTE-TO-F Cdr, CRDEC, AMCCOM ATTN: SMCCR-RSP-A SMCCR-MU SMCCR-MSI

No. of Copies	Organization
1	Director of Defense Research & Engineering ATTN: DD/TWP Washington, DC 20301
1	Assistant Secretary of Defense (Atomic Energy) ATTN: Document Control Washington, DC 20301
1	Chairman Joint Chiefs of Staff ATTN: J-5 (R&D Div) Washington, DC 20301
2	Deputy Chief of Staff for Operations and Plans ATTN: Technical Library Director of Chemical and Nuclear Operations Department of the Army Washington, DC 20310
1	Director Defense Advanced Research Projects Agency ATTN: Tech Lib 1400 Wilson Boulevard Arlington, VA 22209
2	Director Federal Emergency Management Agency ATTN: Public Relations Office Technical Library Washington, DC 20472
1	Director Defense Intelligence Agency ATTN: DT-2/Wpns & Sys Div Washington, DC 20301

No. of Copies	Organization
1	Director National Security Agency ATTN: R15 (E. F. Butala) Ft. George G. Meade, MD 20755
6	Director Defense Nuclear Agency ATTN: CSTI (Tech Lib) DDIR DFSP (Ullrich) NANS OPNA SPSD (Goering/Rohr) TDTR (Kennedy/Hrinishin) Washington, DC 20305
2	Commander Field Command, DNA ATTN: FCPR FCTMOF Kirtland AFB, NM 87115
1	Commander Field Command, DNA Livermore Branch ATTN: FCPRL P.O. Box 808 Livermore, CA 94550
10	Central Intelligence Agency DIR/DB/Standard ATTN: GE-47 HQ Washington, DC 20505

No. of Copies	Organization
3	Director US Army Harry Diamond Labs ATTN: SLCHD-NW-RA (L. Belliveau) SLCHD-NW-P (Gwaltney/Meszaros) SLCHD-TA-L (Tech Lib) 2800 Powder Mill Road Adelphi, MD 20783-1197
1	Commander Armament RD&E Center ATTN: SMCAR-TSS Dover, NJ 07801-5001

No. of Copies	Organization
2	Commander US Army CECOM ATTN: AMSEL-RD AMSEL-RO-TPPO-P Fort Monmouth, NJ 07703-5301
1	Commander CECOM R&D Technical Library ATTN: ASNC-ELC-I-T Myer Center Fort Monmouth, NJ 07703-5301
1	Director US Army Missile and Space Intelligence Center ATTN: AIAMS-YDL Redstone Arsenal, AL 35898-5500
1	Director US Army TRADOC Center - WSMR ATTN: ATAA-SL (Mr. Kirby) White Sands Missile Range, NM 88002-5502

No. of Copies	Organization
1	Commander US Army Foreign Science and Technology Center ATTN: Research & Data Branch 220 7th Street , NE. Charlottesville, VA 22901
1	Commander US Army Logistics Management Center ATTN: ATCL-O (R. Cameron) Fort Lee, VA 23801
1	Commander US Materials Technology Laboratory ATTN: SLCMT-ATL Watertown, MA 02172-0001
1	Commander US Army Strategic Defense Command ATTN: CSSD-H-MPL (Tech Lib) CSSD-H-XM (Dr. Davies) P.O. Box 1500 Huntsville, AL 35807
2	Commander US Army Natick Research and Development Center ATTN: AMDNA-D (Dr. D. Sieling) STRNC-UE (J. Calligeros) Natick, MA 01762
1	Commander US Army Engineer Division ATTN: HNDED-FD P.O. Box 1500 Huntsville, AL 35807
3	Commander US Army Corps of Engineers Waterways Experiment Station ATTN: CAWES-SS-R (J. Watt) CAWES-SE-R (J. Ingram) CAWES-TL (Tech Lib) P.O. Box 631 Vicksburg, MS 39180-0631

No. of Copies	Organization
1	Commander US Army Research Office ATTN: SLCRO-D P.O. Box 12211 Research Triangle Park, NC 27709-2211
3	Commander US Army Nuclear & Chemical Agency ATTN: ACTA-NAW MONA-WE Tech. Lib. 7500 Backlick Rd, Bldg. 2073 Springfield, VA 22150
1	Director HQ, TRAC RPD ATTN: ATRC-RPR (Mr. Radda) Fort Monroe, VA 23651-5143
1	Commander TRADOC Analysis Command ATTN: ATRC Fort Leavenworth, KS 66027-5200
1	Commander US Army Test & Evaluation Command Nuclear Effects Laboratory ATTN: STEWS-TE-NO (Dr. J.L. Meason) P.O. Box 477 White Sands Missile Range, NM 88002
2	Director Joint Strategic Target Planning Staff JCS ATTN: JLTW TPTP Offut AFB Omaha, NB 68113
1	Commandant Interservice Nuclear Weapons School ATTN: Technical Library Kirtland AFB, NM 87115

No. of Copies	Organization
2	Chief of Naval Operations ATTN: OP-03EG OP-985F Department of the Navy Washington, DC 20350
1	Chief of Naval Research ATTN: N. Perrone Department of the Navy Arlington, VA 22217
1	Director Strategic Systems Projects Office ATTN: NSP-43, Tech Library Department of the Navy Washington, DC 20360
1	Commander Naval Electronic Systems Command ATTN: PME 117-21A Washington, DC 20360
1	Commander Naval Facilities Engineering Command ATTN: Technical Library Washington, DC 20360
1	Commander Naval Sea Systems Command ATTN: Code SEA-62R Department of the Navy Washington, DC 20362-5101
5	Officer-in-Charge Naval Construction Battalion Center Civil Engineering Laboratory ATTN: Code L64 (N. P. Clark) Code L54 (R. J. Odello) Code L51 (W. Keenan) Code LO6C/LO8A (Tech Lib) Port Hueneme, CA 93041
1	Commander David W. Taylor Naval Ship Research & Development Command ATTN: Code 522 (Lib Div) Bethesda, MD 20084-5000

No. of Copies	Organization
1	Commander Naval Surface Warfare Center ATTN: Code DX-21 (Library) Dahlgren, VA 22448-5000
1	Officer in Charge White Oak Warfare Center Detachment Code E232 (Tech Library) 10901 New Hampshire Ave Silver Spring, MD 20903-5000
1	Commanding Officer White Oak Warfare Center ATTN: Code WA501 (NNPO) Silver Spring, MD 20902-5000
1	Commander Naval Weapons Center ATTN: Code 533 (Tech Library) China Lake, CA 93555-6001
1	Commander Naval Weapons Evaluation Fac ATTN: Document Control Kirtland AFB, NM 87117
1	Commander Naval Research Laboratory ATTN: Code 2027, Tech Library Washington, DC 20375
1	Superintendent Naval Postgraduate School ATTN: Code 2124, Tech Library Monterey, CA 93940
1	AFSC/SDOA Andrews AFB, MD 20334
2	Air Force Armament Laboratory ATTN: AFATL/DOIL AFATL/DLYV Eglin AFB, FL 32542-5000

No. of Copies	Organization
1	AFESC/RDCS ATTN: Paul Rosengren Tyndall AFB, FL 32403
1	RADC (EMTLD/Docu Library) Griffiss AFB, NY 13441
2	Air Force Weapons Laboratory ATTN: NTES, R. Henny NTED, J. W. Aubrey Kirtland AFB, NM 87117-6008
2	Commander-in-Chief Strategic Air Command ATTN: NRI-STINFO Lib Offutt AFB, NB 68113
1	AFIT ATTN: Tech Lib (Bldg. 640/B) Wright-Patterson AFB, OH 45433
1	FTD/NIIS Wright-Patterson AFB Ohio 45433
1	U.S. Department of Energy Idaho Operations Office ATTN: Spec Programs (J. Patton) 785 DOE Place Idaho Falls, ID 83402
2	Director Idaho National Engineering Laboratory EG&G Idaho Inc. ATTN: Mr. W. C. Reed Mr. T. R. Reed P.O. Box 1625 Idaho Falls, ID 83415
1	Director Lawrence Livermore Lab. ATTN: Tech Info Dept L-3 P.O. Box 808 Livermore, CA 94550

No. of Copies	Organization
2	Director Los Alamos Scientific Lab. ATTN: Doc Control for Rpts Library P.O. Box 1663 Los Alamos, NM 87544
2	Director Sandia Laboratories ATTN: Doc Control 3141 Sandia Rpt Collection L. J. Vortman P.O. Box 5800 Albuquerque, NM 87185-5800
1	Director Sandia Laboratories Livermore Laboratory ATTN: Doc Control for Tech Library P.O. Box 969 Livermore, CA 94550
1	Director National Aeronautics and Space Administration ATTN: Scientific & Tech Info Fac P.O. Box 8757, BWI Airport Baltimore, MD 21240
1	Director NASA-Langley Research Center ATTN: Tech Lib Hampton, VA 23665
1	Director NASA-Ames Research Center Applied Computational Aerodynamics Branch ATTN: MS 202-14, Dr. T. Holtz Moffett Field, CA 94035
3	Applied Research Associates, Inc. ATTN: N.H. Ethridge J. Keefer Library P.O. Box 548 Aberdeen, MD 21001

No. of Copies	Organization
1	Aerospace Corporation ATTN: Tech Info Services P.O. Box 92957 Los Angeles, CA 90009
1	Agbabian Associates ATTN: M. Agbabian 250 North Nash Street El Segundo, CA 90245
1	Applied Research Associates, Inc. ATTN: R. L. Guice 7114 West Jefferson Ave., Suite 305 Lakewood, CO 80235
1	The BDM Corporation ATTN: Richard Hensley P.O. Box 9274 Albuquerque, NM 87119
1	Black & Veach Consulting Engineers ATTN: H. D. Laverentz 1500 Meadow Lake Parkway Kansas City, MO 64114
1	The Boeing Company ATTN: Aerospace Library P.O. Box 3707 Seattle, WA 98124
1	California Research & Technology, Inc. ATTN: M. Rosenblatt 20943 Devonshire Street Chatsworth, CA 91311
1	Carpenter Research Corporation ATTN: H. Jerry Carpenter 27520 Hawthorne Blvd., Suite 263 P. O. Box 2490 Rolling Hills Estates, CA 90274
1	Dynamics Technology, Inc. ATTN: D. T. Hove Suite 300 21311 Hawthorne Blvd. Torrance, CA 90503

No. of Copies	Organization
1	EATON Corporation Defense Valve & Actuator Div. ATTN: Dr. J. Y. S. Yang 2338 Alaska Ave. El Segundo, CA 90245-4896
1	Goodyear Aerospace Corporation ATTN: R. M. Brown, Bldg 1 Shelter Engineering Litchfield Park, AZ 85340
4	Kaman AviDyne ATTN: Dr. R. Reutenick (2 cys) Mr. S. Criscione Mr. R. Milligan 83 Second Avenue Northwest Industrial Park Burlington, MA 01830
3	Kaman Sciences Corporation ATTN: Library P. A. Ellis F. H. Shelton 1500 Garden of the Gods Road Colorado Springs, CO 80907
1	Kaman Sciences Corporation ATTN: Mr. F. W. Balicki 6400 Uptown Boulevard N.E. Suite 300 Albuquerque, NM 87110
2	Kaman-TEMPO ATTN: DASIAC Don Sachs P.O. Drawer QQ 816 State Street Santa Barbara, CA 93102
1	Lockheed Missiles & Space Co. ATTN: J. J. Murphy, Dept. 81-11, Bldg. 154 P.O. Box 504 Sunnyvale, CA 94086
1	Martin Marietta Aerospace Orlando Division ATTN: G. Fotieo P.O. Box 5837 Orlando, FL 32805

No. of Copies	Organization
2	McDonnell Douglas Astronautics Corporation ATTN: Robert W. Halprin K.A. Heinly 5301 Bolsa Avenue Huntington Beach, CA 92647
2	Physics International Corporation 2700 Merced Street San Leandro, CA 94577
2	R&D Associates ATTN: Technical Library Allan Kuhl P.O. Box 9695 Marina Del Rey, CA 90291
1	R&D Associates ATTN: G.P. Ganong P.O. Box 9330 Albuquerque, NM 87119
2	Science Applications, Inc. ATTN: W. Layson John Cockayne PO BOX 1303 1710 Goodridge Drive McLean, VA 22102
1	Science Applications International Corp. ATTN: Mr. J. Guest 2109 Air Park Rd SE Albuquerque, NM 87106
1	Sparta, Inc. Los Angeles Operations ATTN: I. B. Osofsky 3440 Carson Street Torrance, CA 90503
1	Sverdrup Technology, Inc. ATTN: R. F. Starr P. O. Box 884 Tullahoma, TN 37388
1	SRI International ATTN: Dr. G. R. Abrahamson 333 Ravenswood Avenue Menlo Park, CA 94025

No. of Copies	Organization
2	S-CUBED ATTN: C. E. Needham Lynn Kennedy PO Box 8243 Albuquerque, NM 87198
3	S-CUBED ATTN: Technical Library R. Duff K. Pyatt PO Box 1620 La Jolla, CA 92037-1620
1	Texas Engineering Experiment Station ATTN: Dr. D. Anderson 301 Engineering Research Center College Station, TX 77843
1	Thermal Science, Inc. ATTN: R. Feldman 2200 Cassens Dr. St. Louis, MO 63026
1	TRW - Ballistic Missile Division ATTN: H. Korman, Mail Station 526/614 P.O. Box 1310 San Bernadino, CA 92402
1	Battelle Memorial Institute ATTN: Technical Library 505 King Avenue Columbus, OH 43201
1	California Institute of Technology ATTN: T. J. Ahrens 1201 E. California Blvd. Pasadena, CA 91109
2	Denver Research Institute University of Denver ATTN: Mr. J. Wisotski Technical Library PO Box 10127 Denver, CO 80210

No. of Copies	Organization
1	Massachusetts Institute of Technology Aeroelastic and Structures Research Laboratory ATTN: Dr. E. A. Witmer Cambridge, MA 02139
1	Massachusetts Institute of Technology ATTN: Technical Library Cambridge, MA 02139
1	New Mexico Engineering Research Institute (CERF) University of New Mexico ATTN: Dr. J. Leigh P.O. Box 25 Albuquerque, NM 87131
1	Northrop University ATTN: Dr. F. B. Safford 5800 W. Arbor Vitae St. Los Angeles, CA 90045
2	Southwest Research Institute ATTN: Dr. W. E. Baker A. B. Wenzel 8500 Culebra Road San Antonio, TX 78228
1	Stanford University ATTN: Dr. D. Bershader Durand Laboratory Stanford, CA 94305

Aberdeen Proving Ground

Cdr, USATECOM
ATTN.
AMSTE-TE-F (L. Teletski)

Cdr, USATHMA
ATTN: AMXTH-TE

USER EVALUATION SHEET/CHANGE OF ADDRESS

This laboratory undertakes a continuing effort to improve the quality of the reports it publishes. Your comments/answers below will aid us in our efforts.

1. Does this report satisfy a need? (Comment on purpose, related project, or other area of interest for which the report will be used.) ______________________________

2. How, specifically, is the report being used? (Information source, design data, procedure, source of ideas, etc.) ______________________________

3. Has the information in this report led to any quantitative savings as far as man-hours or dollars saved, operating costs avoided, or efficiencies achieved, etc? If so, please elaborate. ______________________________

4. General Comments. What do you think should be changed to improve future reports? (Indicate changes to organization, technical content, format, etc.) ______________________________

BRL Report Number ______________ Division Symbol ______________

Check here if desire to be removed from distribution list. ____

Check here for address change. ____

Current address: Organization ______________________
Address ______________________

-----------------------------FOLD AND TAPE CLOSED-----------------------------

Director
U.S. Army Ballistic Research Laboratory
ATTN: SLCBR-DD-T(NEI)
Aberdeen Proving Ground, MD 21005-5066

OFFICIAL BUSINESS
PENALTY FOR PRIVATE USE $300

NO POSTAGE NECESSARY IF MAILED IN THE UNITED STATES

BUSINESS REPLY LABEL
FIRST CLASS PERMIT NO. 12062 WASHINGTON D C

POSTAGE WILL BE PAID BY DEPARTMENT OF THE ARMY

Director
U.S. Army Ballistic Research Laboratory
ATTN: SLCBR-DD-T(NEI)
Aberdeen Proving Ground, MD 21005-9989